Università degli Studi di Ferrara
Facoltà di Scienze Matematiche Fisiche e Naturali

Dipartimento di Fisica

Dottorato di Ricerca in Fisica, XVI ciclo

Data Analysis of a coherent network of gravitational wave detectors

Ph. D. Student: **Francesco Salemi**

Supervisor: Prof. **Pierluigi Fortini**

In theory, there is no difference between theory and practice.
In practice, there is.

Yogi Berra

Contents

1 Resonant gravitational waves detectors **3**

1.1 A brief overview on gravitational waves 3

1.2 Recent upgrades of AURIGA detector and near future prospects . . 4

1.2.1 AURIGA second run model 8

1.2.2 Comparison with other g.w. experiments: design and current sensitivity curves 9

1.2.3 AURIGA Status 10

2 G.W. Burst Sources **15**

2.1 Supernova rotational core collapse 15

2.1.1 MPA Newtonian and Relativistic templates 16

2.1.2 Estimating SNR for AURIGA detector 18

2.2 Coalescing Binaries 22

2.2.1 Inspiral 22

2.2.2 Merger 23

2.2.3 Ringdown 23

2.3 Gamma-ray Burst Models 24

3 Single detector estimation methods **27**

3.1 The AURIGA Matched Filter 28

3.1.1 Timing errors, bias on the SNR and ROCs 29

3.2 Maximum Likelihood Estimators of Signal Parameters 33

3.3 Excess Power through Karhunen-Loève Expansion 34

3.3.1 Statistical analysis 36

3.3.2 Timing errors and bias on SNR 37

3.4 Error Bounds 39

3.4.1 Cramèr-Rao Lower Bound 39

3.4.2 Weiss-Weistein Lower Bound 41

4 Methods of gw network data analysis **43**
4.1 Coincident trigger search 44
4.2 Externally triggered search 46
4.3 Cross correlation 47
4.4 Coherent network search 48
4.4.1 Network geometry 48
4.4.2 Template-based search 49
4.4.3 Non-Template search method 52
4.5 Summary and Discussion 53

5 Conclusions and perspectives **55**

A ROC (Receiver Operating Characteristic curves) **57**

B Karhunen-Loève expansion **59**
B.1 Introduction 59

Introduction

A great part of what we know about the Universe passes through the observation of electromagnetic waves: from radio waves up to γ rays. Some complementary information comes from the detection of cosmic rays and neutrinos, that allow for different perspectives on our Universe. Similarly, gravitational wave astronomy might increase considerably our knowledge and allow the comprehension of the most violent and catastrophic events occurring in the nearby Universe.

Whereas light or matter waves propagate through space, gravitational waves are propagating ripples of spacetime itself. Such distortions in spacetime are generated by non-spherical motion of matter. There are large uncertainties in the theoretical predictions of either the strength or the rate of occurrence of gravitational wave (gw) events, in the ranges of strengths and frequencies under observation by present gw detectors. In most cases, theory can only give an indication on which gw sources might be promising and suggests estimates on the energy emitted in gws and event rates. The first raw information drawn from models is that even the most violent astrophysical phenomena involving compact objects such as merging black holes or neutron stars, or collapsing stars, emit gravitational waves which manifest themselves as a tiny relative shift of only $\Delta l/l \sim 10^{-20}$ on the Earth.

Although gravitational waves have been predicted by Albert Einstein in his theory of general relativity over 80 years ago, only nowadays technology enables physicists to tackle the problem of their detection. A successful detection of gravitational waves will not only supply a further confirmation to Einstein's prediction, but will open a completely new "window" into the Universe. By routinely observing gravitational waves, astrophysicists will gain new, and otherwise entirely unattainable insights, into such fascinating objects like black holes, the enigmatic cosmic gamma ray bursts, or the driving engines behind stellar supernova explosions [30].

Since the well known observations made by Hulse and Taylor (1994) of the binary system PSR1913+16 [1, 2], the scientific community is waiting for the day in which a detector, or most likely a network of detectors, will claim the first *direct* observation of a gravitational signal. Note that this enthusiasm was triggered by

a source that actually is not very promising, neither for the energy radiated in gw nor for the expected rate of occurrence.
More recently (December 2003), a revised estimate of the neutron-star merger rate has been assessed through the discovery of a double neutron-star system, a pulsar called PSR J0737-3039 and its neutron-star companion, by a team of scientists from Italy, Australia, the UK and the USA using the 64-m CSIRO Parkes radio telescope in eastern Australia [3].
The challenge of detecting gws was firstly addressed by Joseph Weber, who is generally considered the pioneer of this field. Using room-temperature aluminum bars as detectors, he reported tentative evidences for gw bursts at the kHz frequencies (1969). This first report, although later on denied by more sensitive detectors, has triggered considerable efforts in this direction, giving birth to a new field of astrophysical detection.
There are five operating resonant gw detectors: ALLEGRO [4] in Baton Rouge (USA), AURIGA [5] in Legnaro, near Padova (Italy), EXPLORER [6] in CERN (Switzerland), NAUTILUS [7] in Frascati, near Rome (Italy) and NIOBE [8] in Perth (Australia).
The five detectors have signed the International Gravitational Event Collaboration (IGEC) [9], with the purpose of data exchange and coincidence searching among different detectors. This joint effort led to an upper limit on the gws from the galactic center [10], and showed that the data exchange technique allows to make the false alarm rate negligible [10].

Another way to search for gws is by interferometric experiments.
In 1978, Forward made the very first experimental attempt to detect gws by means of an interferometer, measuring the displacement of test masses with high sensitivity. Since then, the sensitivity of such detectors has greatly increased, following a thorough test of several optical schemes.
There are currently four (actually five counting the two sites of LIGO) interferometric gw detectors: GEO 600 [11] in Hannover (Germany), LIGO Hanford and LIGO Livingston in the USA [12], TAMA 600 [13] in (Japan) and VIRGO [14] in Cascina, near Pisa (Italy). They are now constantly upgrading, both as regards sensitivity and duty cycle, struggling to reach their goal sensitivity curves.

In the future there will also be LISA [15], the ESA-NASA collaboration to bring the gw research into the space, where the detection of the gw should be out of doubt, as it is limited to the lowest range of frequencies.

The detection of an event in a single detector is not sufficient to claim any discovery: a multi-detector search has to be performed to reach a sufficient level

of confidence for the detection.
The aim of this work is to develop multi-detector data analysis techniques. However, before analyzing a network of detectors, part of the work was devoted to the study of two different types of analysis, which have been implemented in AURIGA data analysis. As described in chapter 3, the standard AURIGA data analysis corresponds to an event search on template-filtered data and to a template-less event search, based on the Excess Power method [53]. These two event search pipelines are compared as regards to their parameters estimation capabilities and the False Alarms and False Dismissals probabilities. In addition, theoretical lower bounds on parameter estimation errors are recalled to give some additional insight in the estimators performances. Chapter 4 deals with the multi-detector analysis and the various methods of combining data from different detectors; part of this chapter comes from a paper published on the proceedings of GWDAW2002 [75].
Chapter 1 gives a brief overview on the detector AURIGA, as regards its recent hardware and software upgrades, and shows the theoretical and experimental sensitivity curves of other gw detectors as a comparison.
Chapter 2 covers the main astrophysical sources which should be relevant to resonant detectors.

Chapter 1

Resonant gravitational waves detectors

1.1 A brief overview on gravitational waves

Resonant gravitational waves (gw) detectors are massive mechanical oscillators, equipped with very sensitive displacement sensors, capable of detecting changes in the vibrational amplitude of the oscillator motion. The displacement sensitivity of a resonant detector is of the order of 10^{-21} m for short transients ($\Delta t \lesssim 1$ s), level at which an excitation due to the interaction of gw with the bar should emerge from the detector noise.

Gravitational signals should come from astrophysical objects experiencing extreme conditions, in which the effects of the Einstein theory of General Relativity (GR) [21] allow huge quantity of energy ($\approx 1 M_{\odot} \simeq 10^{53}$ erg) to be converted in spacetime perturbations travelling through the universe and finally reaching the earth.

A formula for the total *luminosity* emitted by a gw source is available in the weak-field limit [1] [22]:

$$L_g \;=\; \left(\frac{dE}{dt}\right) \;=\; \frac{G}{5c^5}\Sigma_{i,j}\left(\frac{d^3 Q_{ij}^{TT}}{dt^3}\right)^2 , \tag{1.2}$$

where G is the Newton gravitational constant, c is the speed of light and Q_{ij}^{TT}

[1] In the weak-field limit the metric tensor $g_{\mu\nu}$ is quasi-minkowskian:

$$g_{\mu\nu} \;=\; \eta_{\mu\nu} + h_{\mu\nu} , \qquad |h_{\mu\nu}| \ll 1 \tag{1.1}$$

are the elements of the quadrupolar tensor for the mass distribution of the source, calculated in the Transverse Traceless gauge:

$$Q_{ij}^{TT}(t) \;=\; \left(\int_V \rho(\mathbf{x},t)\left(x_i x_j - \frac{1}{3}\delta_{ij}|\mathbf{x}|^2\right) dV\right)^{TT}. \tag{1.3}$$

The expression for the perturbation of the metric tensor in the wave region is [23]:

$$h_{ij} \;=\; \frac{1}{r}\frac{2G}{c^4}\frac{d^2 Q_{ij}^{TT}(t-r/c)}{dt^2}, \tag{1.4}$$

where r is the distance of the observer from the source.
Eq.(1.3) can be used to give a rough estimate of the luminosity of an astrophysical source:

$$L_g \sim \varepsilon^2 \frac{G}{c^5}\frac{M^2 R^4}{T^6}. \tag{1.5}$$

where M, R and T are its mass, its radius and the characteristic evolution time of the source, respectively; ε is a measure of the asymmetry of the matter distribution. Accordingly, the amplitude of metric perturbation h reads:

$$h \sim \frac{G}{c^4}\frac{E^{\rm ns}}{r}, \tag{1.6}$$

where $E^{\rm ns} = \varepsilon M R^2/T^2$ is the source energy (proportional to the fraction of matter which is *not spherically* symmetric).
The factor G/c^5 keeps the luminosity so small that we must look for massive and compact objects, in relativistic motion. The luminosity can be rewritten as:

$$L_g \sim \frac{c^5}{G}\left(\frac{r_s}{R}\right)^2\left(\frac{v}{c}\right)^6, \tag{1.7}$$

where R and v are respectively the typical scale of the source and velocity of the system, $r_s = 2GM/c^2$ is the Schwarzschild radius.

For the most luminous gw sources, the weak-field approximation no longer holds ($r \to r_s$ and $v \to c$) and therefore, efforts to build reliable theoretical models are of paramount importance [30, 31]. Accurate numerical simulations for the full 3-D general relativistic problem [38] should predict the range of frequencies for the design of new detectors and signal templates to be used in the data analysis.

1.2 Recent upgrades of AURIGA detector and near future prospects

The first run of gw detector AURIGA began on June 1997 and ended in November 1999 because of a cryogenic failure, which forced the warm up of the detector at

room temperature.
During the two years of data acquisition, the detector operated at a minimum thermodynamic temperature of 200 mK, reaching the best strain sensitivity of $S_{hh}^{1/2} \simeq 4 \times 10^{-22}$ Hz$^{-1/2}$ over a a bandwidth of ~ 1 Hz around the two resonant frequencies [16]. It is worth noticing that also the achieved duty cycle (30%) was unsatisfactory since we are looking for rare astrophysical sources.
Since the end of previous run, the group has been working on the upgrade of the whole project AURIGA [17].

In order to perform all the measurements necessary to fully characterize the new AURIGA readout, a specific apparatus, the Transducer Test Facility (TTF) [20], was set up. In the TTF, shown in figure 1.1, the transduction chain is identical to the one mounted on the gw detector.

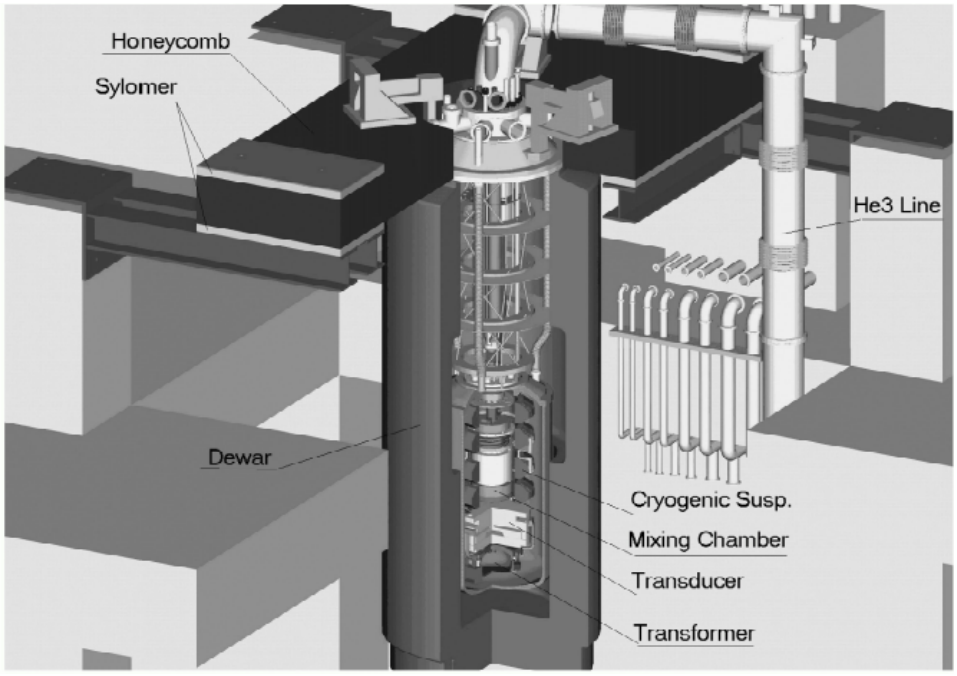

Figure 1.1: Cross section of the Transducer Test Facility: the cryostat, the structure of the multi-stage suspension system, and the resonant transducer. The box attached to the last stage of the suspensions contains the double SQUID amplifier.

TTF allows frequent ultra-cryogenic measurements on the complete readout chain as its cryogenic time to cool down or heat up is less than one week, while the AURIGA cryogenic time is of the order of one month. Once the readout has shown to work properly, it has been installed on the AURIGA bar. In figure 1.2

there is a picture of the open cryostat, in the assembling phase of AURIGA detector (October 2003).

The ultra-cryogenic detectors achieve a better sensitivity with respect to detectors operated at liquid Helium temperature, but the dilution refrigerator shrinks the duty cycle and reduces the system's reliability. Consequently, it has been decided to split the second run into two phases: a first phase, which is currently taking place, where the detector is operating at cryogenic temperature ($T_{therm} \sim 4.5 - 1.5$ K) and a second phase, with a new designed ^{3}He-^{4}He dilution refrigerator to reach lower temperatures ($T_{therm} \sim 0.1$ K) and the better sensitivities (see figure 1.4).

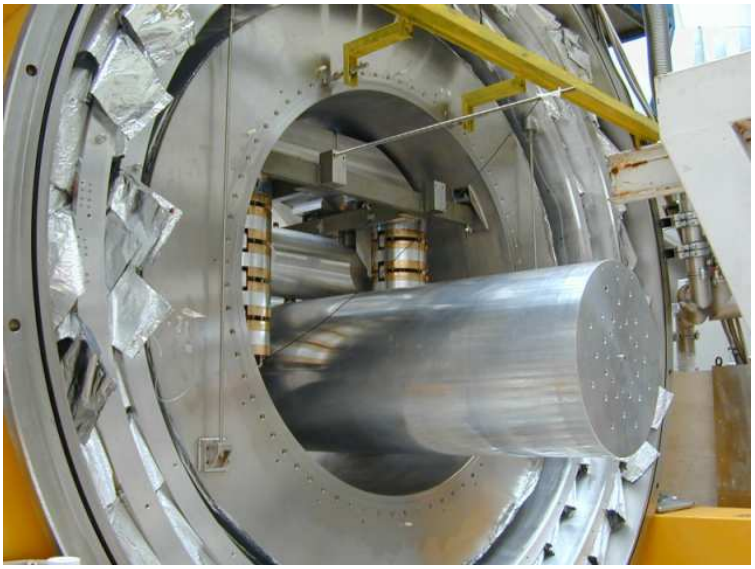

Figure 1.2: A picture of AURIGA detector with the new multistage suspensions.

In the second run, the AURIGA detector has been equipped with:

- new mechanical suspensions designed by means of a Finite Element Method (FEM) to avoid spurious mechanical resonances in the detector bandwidth: attenuation $>$ 360 dB at 1 kHz (see figure 1.3)
- new capacitive transducer: two modes (1 mechanical+1 electrical)
- new amplifier: double stage SQUID with 200$\hbar$ energy resolution
- new data analysis: C++ object oriented code and frame data format.

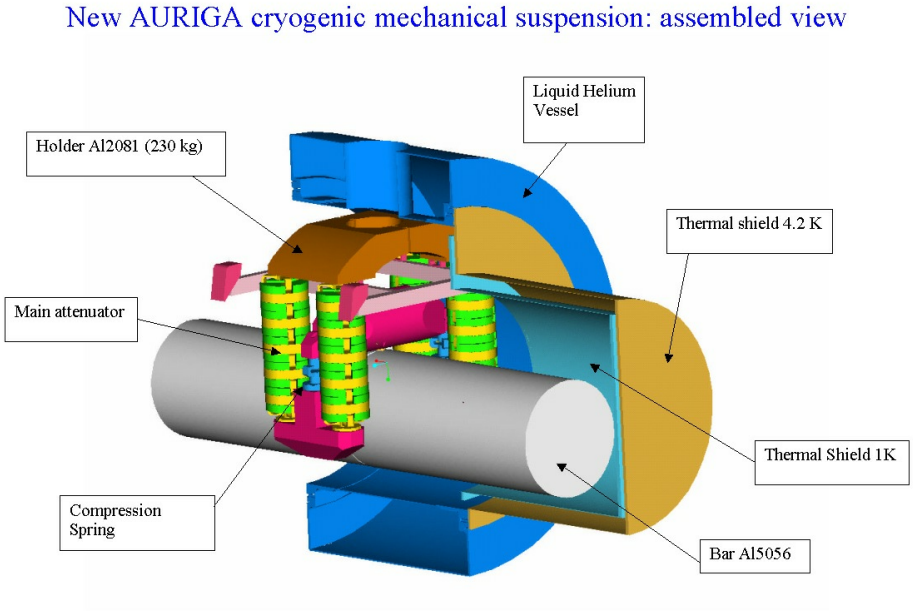

Figure 1.3: A close view of AURIGA new suspensions: the 4K vessel of the cryostat supports a stainless steel frame, to which the whole suspension system is hung. The four main suspension columns are fixed to a big 300 kg aluminum mass holder, supported by four titanium springs. The aim of these four springs is to uncouple the steel frame from the columns. Each pair of columns supports an inverted "T" aluminum mass on the top of which is fixed a compression spring with an upper conical joint which is used to lean an aluminum beam. The bar is hung at its center of mass with a tubular cable which is attached with a "bayonet" mount into the aluminum beam.

To satisfy the new requirements of the improved detector design, (i.e. the wider bandwidth and the higher sensitivity), the data acquisition and data analysis systems have been fully redesigned and implemented *from scratch* [19].

Operating gw detectors in a coordinated network allows for a drastic reduction of spurious signals and an experimental determination of the false alarm rate. To this end a great effort has been put to reach an accurate data synchronization with the Universal Time Coordinate (UTC) and permanent and temporary data storage has been based on the Frame format [2].

[2]The Frame format [24] has been developed by VIRGO and LIGO groups and adopted by the gravitational wave community.

1.2.1 AURIGA second run model

Within a 200 Hz bandwidth centered around the mode frequencies $\approx [800 \div 1000]$ Hz , resonant detectors are well described by linear, constant coefficients differential equations, so that both the detector transfer function $H(\omega)$, and the noise spectral density $S(\omega)$, can be reasonably well approximated by real coefficient polynomials. A suitable model of the power spectrum of the AURIGA noise and the detector transfer function are the complex zeroes-poles functions derived in ref. [47]

$$S(\omega) \equiv L(i\omega)L(-i\omega) = S_0 \prod_{k=1}^{N_P} \frac{(q_k + i\omega)(q_k - i\omega)(q_k^* + i\omega)(q_k^* - i\omega)}{(p_k + i\omega)(p_k - i\omega)(p_k^* + i\omega)(p_k^* - i\omega)}, \tag{1.8}$$

and

$$H(\omega) = H_0(\omega) \ \frac{(-i\omega)^{N_P+2}}{\prod_{k=1}^{N_P}(p_k - i\omega)(p_k^* - i\omega)} \ , \tag{1.9}$$

where S_0 is a constant representing the wide-band noise level, N_P is the number of resonances (in our case the system can be modelled with $N_P = 3$), p_k and q_k are respectively the poles and the zeroes (see tables 1.1 and 1.2) and $H_0(\omega)$ is the calibration function that has to be provided by the detector calibration procedures at any run and monitored during the data taking. The poles p_k entering in Eq.s 1.8 and 1.9 are subject to slow drifts mainly caused by discharges of the capacitive transducer or variations of the thermodynamic temperature (usually less than few mHz per month).

p_1	$-0.409 + i5421.781$ [rad/s]
p_2	$-3.469 + i5780.161$ [rad/s]
p_3	$-8.781 + i5996.345$ [rad/s]
q_1	$-1653.439 + i5345.336$ [rad/s]
q_2	$-47.980 + i5445.167$ [rad/s]
q_3	$-50.393 + i5842.61$ [rad/s]

Table 1.1: Parameters for the noise model of AURIGA second run phase I at 4.5 K.

From the previous equations is straightforward to obtain the modelled $S_{hh} \equiv S(\omega)/|H(\omega)|^2$ strain sensitivity for the two devised phases shown in figure 1.4.

p_1	$-0.409 + i5421.781$ [rad/s]
p_2	$-3.469 + i5780.161$ [rad/s]
p_3	$-8.781 + i5996.345$ [rad/s]
q_1	$-42.838 + i5437.447$ [rad/s]
q_2	$-683.443 + i5824.997$ [rad/s]
q_3	$-52.716 + i5840.513$ [rad/s]

Table 1.2: Parameters for the noise model of AURIGA second run phase II at 100 mK

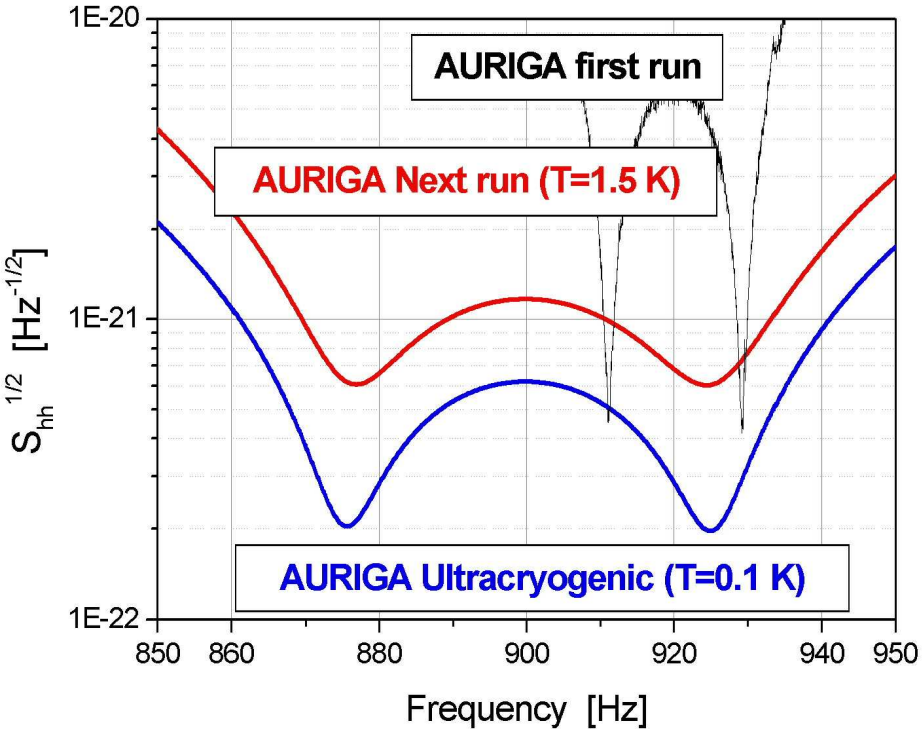

Figure 1.4: Comparison among the sensitivities of the various hardware setups of AURIGA: i) a S_{hh} from the first run data acquisition (black), ii) design sensitivity of Phase 1 at cryogenic thermodynamic temperatures (red) and iii) design sensitivity of Phase 2 at ultra-cryogenic thermodynamic temperatures (blue)

1.2.2 Comparison with other g.w. experiments: design and current sensitivity curves

The main task to be accomplished by the new AURIGA detector is to exchange data with other gw experiments. It is worth giving a look at the planned (and the

actually reached) sensitivity curves of the operating interferometers. For the sake of simplicity, we choose to omit any resonance, such as violin modes, mirror modes etc. in the detection bandwidth and to consider only the thermal (pendulum and mirror substrates) and the shot noise: the simplified model is therefore [49],

$$S_n(\omega) = \frac{S_{pend}}{\omega^5} + \frac{S_{mirror}}{\omega} + S_{shot}\left[1 + \left(\frac{\omega}{\omega_{knee}}\right)^2\right] \tag{1.10}$$

where S_{pend} and S_{mirror} are the thermal noises of the mirror pendular mode and of the mirror substrates; S_{shot} and ω_{knee} fit the optical read-out noise.

Detector	S_{pend}	S_{mirror}	S_{shot}	$\omega_{knee}/(2\pi)$ [Hz]
GEO	$4.1 \cdot 10^{-32}$	$5.7 \cdot 10^{-42}$	$1 \cdot 10^{-44}$	577
LIGO 2K	$2.1 \cdot 10^{-31}$	$1.4 \cdot 10^{-42}$	$4.35 \cdot 10^{-46}$	182
LIGO 4K	$5.6 \cdot 10^{-32}$	$24.5 \cdot 10^{-43}$	$1.1 \cdot 10^{-46}$	83
TAMA	$4.6 \cdot 10^{-33}$	$3.2 \cdot 10^{-33}$	$1.78 \cdot 10^{-44}$	500
VIRGO	$9 \cdot 10^{-33}$	$28.3 \cdot 10^{-42}$	$3.24 \cdot 10^{-46}$	500

Table 1.3: Parameters for the simplified noise model of the interferometers.

We report the numerical values taken from [49] [3] that fit the model and in figure 1.5 the design sensitivity curves of the five interferometers, compared with the one of AURIGA second run phase 2. Of course, this is an oversimplified comparison: there are other parameters to be taken care of, such as the effective detection bandwidth, the duty cycle, the degree of stationarity, the lock time, the spurious lines etc. Besides, the actual sensitivity curves shown in figures 1.6 and 1.7 of the interferometers that have had science runs (the LIGOs and TAMA interferometers) are still well above the designed ones.

1.2.3 AURIGA Status

On December 2003, the AURIGA detector reached a set of parameters suitable for tests and operation. Data taking began at 4.5 K for diagnostics and calibration. Since December the 24^{th} both the noise floor and the bandwidth have been in close agreement with the performance predicted by the thermodynamic model of the

[3] The sensitivity of GEO600 refers to the wideband configuration. The TAMA detector parameters have been updated to the sensitivity enhancement due to the power recycling upgrade.

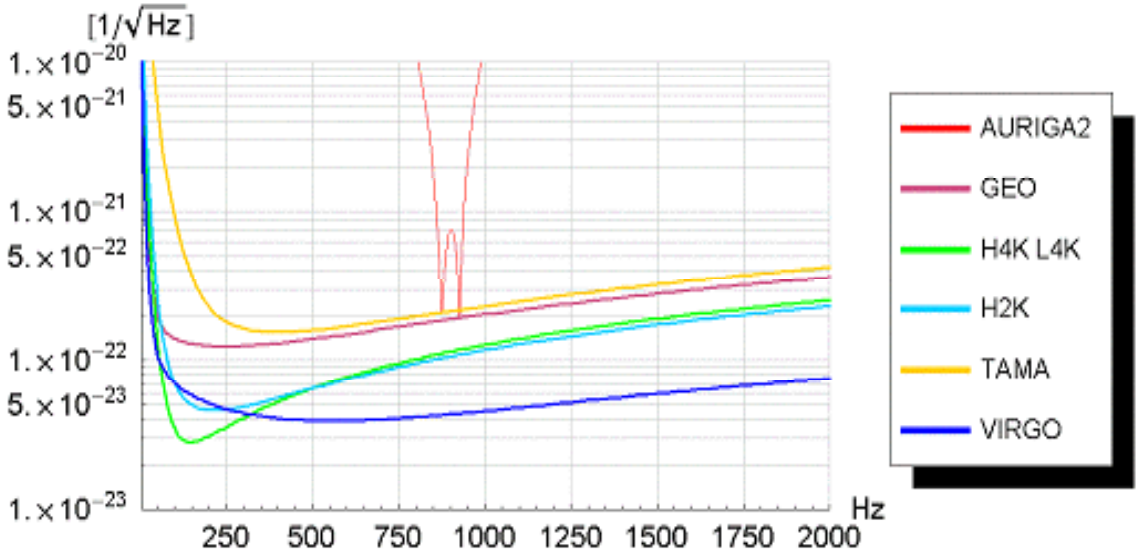

Figure 1.5: Design strain sensitivities of gw detectors. H4K and H2k are, respectively the 4 km and 2 km Hanford interferometer. L4K is the Livingstone 4 km interferometer.

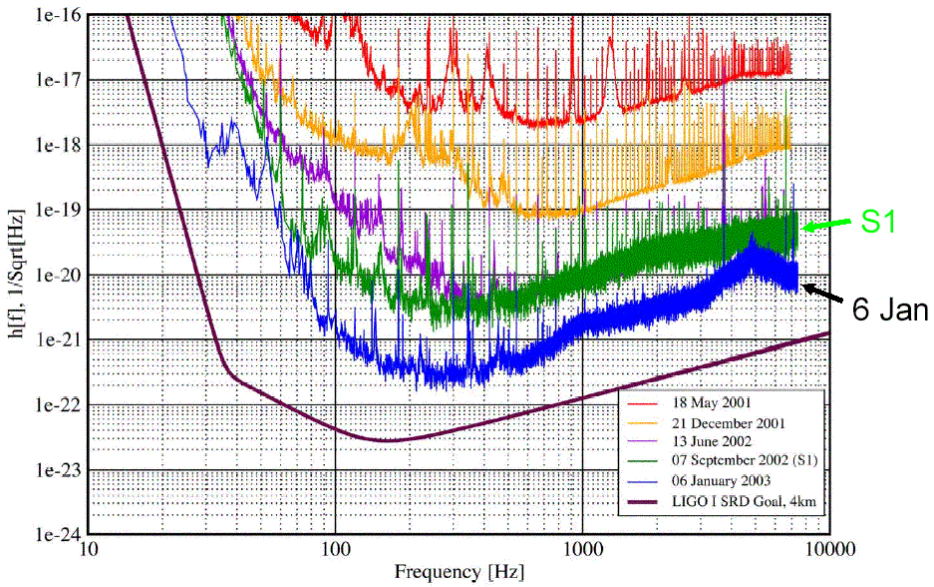

Figure 1.6: Strain sensitivities of LIGO Livingstone 4km.

detector. In particular, the bilateral spectral strain noise is lower than 5×10^{-21} $\mathrm{Hz}^{-1/2}$ between 855 and 950 Hz (see figure 1.8). However, a few spurious non-modelled lines are still present.

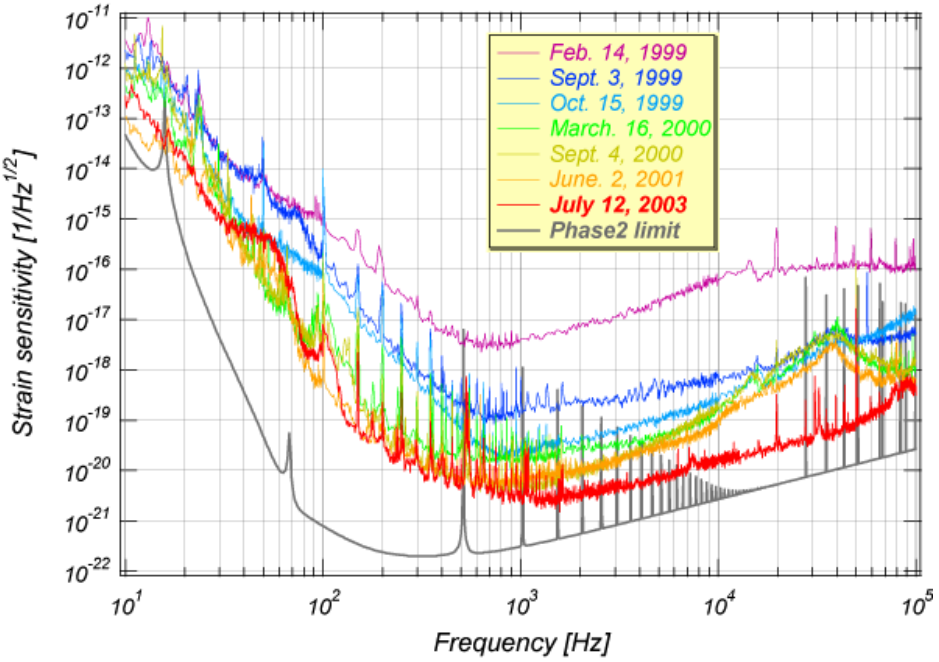

Figure 1.7: Strain sensitivities of Tama300.

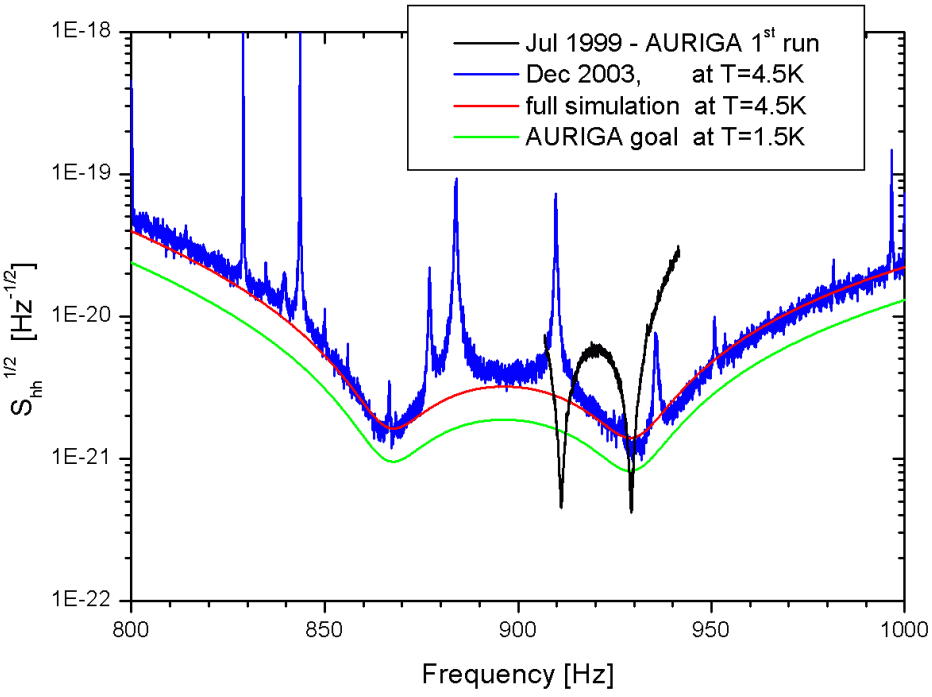

Figure 1.8: Shh of AURIGA second run

Chapter 2

G.W. Burst Sources

In this chapter, we will give a brief introduction to some gw sources. We have chosen the most commonly discussed astrophysical models: supernovae, binary systems and Gamma-Ray Bursts (GRB) sources. Of course, at present such models can only give some indications about the strength and, sometimes, the rate of certain gw events; nevertheless, these are the first steps toward a better comprehension of some of the most intriguing phenomena of the Universe. It's still not clear whether the implementation of new and more accurate relativistic simulations will help us to achieve higher degrees of confidence in theoretical predictions. Probably, this ambiguity will persist till the gw detectors will reach a sensitivity high enough to enlighten the situation.

2.1 Supernova rotational core collapse

At the end of their evolution, massive stars ($M > 4M_{\odot}$) develop an iron core which becomes unstable against gravitational collapse. This core collapses to a neutron star or a black hole releasing gravitational binding energy, which is enough to power a supernova explosion. As the core collapses, large amounts of mass ($1 - 100\ M_{\odot}$) flow in a compact region ($10^8 - 10^9$ cm) at relativistic velocities ($v/c \sim 1/5$). If the collapse is nonspherical, part of this huge energy will be emitted in the form of gravitational waves. For these reasons supernovae have always been considered as one of the most promising sources of gravitational waves; indeed, in the 60's-70's, the first gw detectors - resonant bars - had their resonant frequencies tuned around 1 kHz, in order to look for the typical frequencies expected for these gw signals. However, according to present knowledge, the energy released in gw in rotational core collapse was overestimated by orders of magnitude; a clear upper bound for

this quantity is $E_{gw} \leq 10^{-6} M_{\odot} c^2$ [25]. In supernova core collapse, there are several mechanisms of wave emission (of comparable strength) [30], [29]:

- Deceleration of bulk mass at core bounce (burst signal);
- Bar instability, in which the mass in the core forms a rapidly rotating bar-like structure with a rapidly varying quadrupole moment (quasi-periodic signal);
- Fragmentation instability: the collapse material fragments into clumps, which orbit for some cycles as the collapse proceeds;
- R-modes instability, peculiar of the neutron stars;
- Ring-down signal from a possible newborn black hole: large amounts of material accreting a black hole formed in core collapse would induce a distortion in the Black Hole (BH) stationary Kerr configuration.

The frequency of the emitted radiation ranges from a few Hz to a few kHz and the dimensionless signal amplitudes for a source located at a distance of 10 Mpc do not exceed $h \sim 10^{-22}$: consequently, the prospects of detecting a gw signal from a supernova core collapse by the detectors currently in data taking (and even with next generation detectors) appears to be limited to those events occurring within the Local group (≈ 4 Mpc).

2.1.1 MPA Newtonian and Relativistic templates

At present, one of the most accurate simulations of star collapse has been implemented by a group from the Max-Planck-Institut für Astrophysik. They have performed hydrodynamical simulations of rotational core collapse in axisymmetry and equatorial symmetry: first in the Newtonian approximation [26] and later with a fully relativistic treatment [27], [28]. Note that, at the rotational speeds expected from stellar evolution models, bar-modes do not develop and the dominant gw signal occurs at bounce. This is due to the convection and the viscosity which carry away this already small angular momentum.
To reduce the complexity of the problem, they assume rotating $\gamma = 4/3$ polytropes in equilibrium as initial models of the type iron core, with initial central density $\varrho_c = 10^{10}$ g·cm^{-3}, a radius $R_{core} \sim 1500$ km and a simplified ideal fluid equation of state.
The MPA group has simulated, both in Newtonian and in relativistic gravity, the evolution of 26 models that cover a 3-D parameter space: the first parameter A,

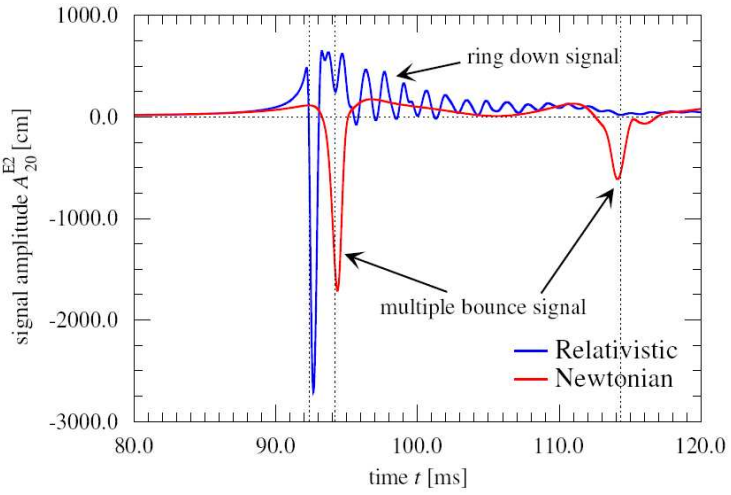

Figure 2.1: Time evolution of the gravitational wave signal Amplitude for the newtonian (red) and the relativistic (blue) simulation of model A3B3G1: while the newtonian simulation has given raise to multiple bounces, the relativistic shows a *regular* collapse.

	A $[cm]$	B	G
1	$5 \cdot 10^9$	0.25%	1.325
2	10^8	0.5%	1.320
3	$5 \cdot 10^7$	0.9%	1.310
4	10^7	1.8%	1.300
5	-	4%	1.280

Table 2.1: The three model parameters. The name of each model is obtained with a combination of parameters from the three sets (i.e. A1B2G3).

is a length scale ranging from $(10^7 \div 5 \times 10^9)$ cm, which specifies the degree of differential rotation. The second parameter B, is the initial rotation rate, i.e. the ratio of rotational energy and the absolute value of gravitational binding energy, spanning from 0.25% to 4%. Finally, the third parameter G is related to the adiabatic index at subnuclear densities: collapse begins as the adiabatic index decreases from 4/3 to G (see Table 2.1).
Three types of rotational supernova core collapse and related waveforms have been identified in both set of simulations: regular collapse, multiple bounce and rapid collapse.

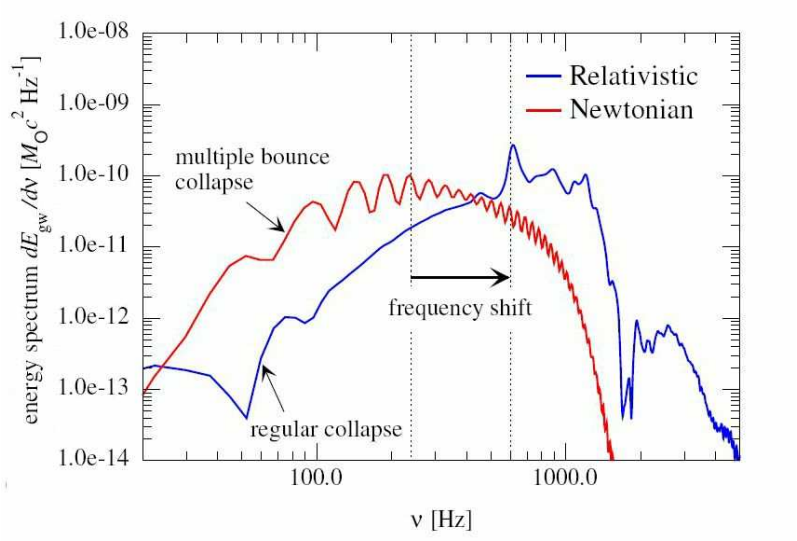

Figure 2.2: Spectral energy distribution of gw signal for the newtonian and the relativistic simulations of model A1B3G3: due to higher average central densities in relativistic simulations, the maximum of the energy spectrum is shifted to higher frequencies.

In figure 2.1, a quick comparison of the Newtonian and the relativistic simulations results is shown. For model A3B3G1, simulations produce very different waveforms: in particular, a *multiple bounce* type (Newtonian) becomes a *regular* one with a ringdown. The range of gw amplitudes and frequencies ν obtained for the two sets is roughly the same: $4\times10^{-21} \leq h^{TT} \leq 3\times10^{-20}$ for a source at a distance of 10 kpc and 60 Hz $\leq \nu \leq$ 1000 Hz. These simulations give an even more restrictive limit with respect to theoretical predictions to the total energy radiated in gw, reduced to only a few $10^{-7}M_{\odot}c^2$. Besides, the relativistic models, that are expected to be more accurate, have typically lower gw amplitudes. Nevertheless, the peak of emission in latter models is at higher frequencies and in some cases very close or inside the bandwidth of the future detector AURIGA2, leading to an SNR enhancement with respect to Newtonian models (see figure 2.2).

2.1.2 Estimating SNR for AURIGA detector

The AURIGA data analysis allows for optimal filtering of arbitrary waveforms; nevertheless, applying a δ-filtering to estimate the SNR and the time of arrival of newtonian and relativistic waveforms is still a good approximation. In fact the response to the major part of the MPA signals is almost flat over the AURIGA bandwidth.

The fraction of in-band SNR ΔSNR/SNR, lost because of the filter mismatch, is lower than 5% if the in-band SNR of injection is larger than 6-7, i.e. in the linear estimation region of the WK delta filter. Note that this result is model dependent: slightly changing AURIGA resonant frequencies of $20-30$ Hz can produce on some MPA waveforms a loss of $20 \div 30\%$ for in-band SNR. These values agree perfectly with those estimated analytically by means of the Fitting Factor (FF) [1] reported on tables 2.2 and 2.3.

[1]The Fitting Factor represents the loss fraction of SNR due to the mismatch between the filter and the actual gw waveform:

$$FF = \frac{(H|T)}{\sqrt{(H|H)}\sqrt{(T|T)}}, \tag{2.1}$$

where $(x|y)$ is the usual scalar product, H is the gw waveform and T the template to whom the filter is matched: in our case the delta function.

	Model	SNR (10 kpc)	Total Energy ($M_\odot c^2$)	h_{TTmax}	FF	T (ms)
1	$A1B1G1_N$	0.80	$5.8 \cdot 10^{-8}$	$1.5 \cdot 10^{-20}$	0.97	108.7
2	$A1B2G1_N$	1.1	$6.4 \cdot 10^{-8}$	$2.1 \cdot 10^{-20}$	1.	112.2
3	$A1B3G1_N$	0.28	$1.8 \cdot 10^{-8}$	$1.3 \cdot 10^{-20}$	0.97	134.7
4	$A1B3G2_N$	1.1	$5.8 \cdot 10^{-8}$	$1.8 \cdot 10^{-20}$	0.99	113.8
5	$A1B3G3_N$	1.1	$2.5 \cdot 10^{-8}$	$8.6 \cdot 10^{-21}$	1.	69.39
6	$A1B3G5_N$	0.45	$3.8 \cdot 10^{-10}$	$1.2 \cdot 10^{-21}$	0.97	58.69
7	$A2B4G1_N$	0.0068	$5.9 \cdot 10^{-10}$	$5.8 \cdot 10^{-21}$	1.	198.2
8	$A3B1G1_N$	1.9	$8.7 \cdot 10^{-8}$	$2.2 \cdot 10^{-20}$	0.95	114.2
9	$A3B2G1_N$	0.70	$2.3 \cdot 10^{-8}$	$1.5 \cdot 10^{-20}$	0.99	133.8
10	$A3B2G2_N$	1.7	$7.6 \cdot 10^{-8}$	$2.1 \cdot 10^{-20}$	0.99	99.12
11	$A3B2G4_N$	1.2	$1.5 \cdot 10^{-8}$	$6.2 \cdot 10^{-21}$	1.	59.68
12	$A3B2G4_s$	1.4	$1.9 \cdot 10^{-8}$	$6.9 \cdot 10^{-21}$	1.	59.63
13	$A3B3G1_N$	0.023	$3.7 \cdot 10^{-9}$	$9.6 \cdot 10^{-21}$	0.94	135.5
14	$A3B3G2_N$	0.23	$9.2 \cdot 10^{-9}$	$1.3 \cdot 10^{-20}$	0.98	106.0
15	$A3B3G3_N$	1.0	$2.1 \cdot 10^{-8}$	$1.3 \cdot 10^{-20}$	0.95	77.09
16	$A3B3G5_N$	0.76	$2.7 \cdot 10^{-9}$	$2.3 \cdot 10^{-21}$	0.99	57.07
17	$A3B4G2_N$	0.040	$1.5 \cdot 10^{-9}$	$7.9 \cdot 10^{-21}$	1.	117.4
18	$A3B5G4_N$	0.018	$1.1 \cdot 10^{-9}$	$4.7 \cdot 10^{-21}$	0.95	88.40
19	$A4B1G1_N$	1.8	$6.9 \cdot 10^{-8}$	$1.8 \cdot 10^{-20}$	0.89	118.9
20	$A4B1G2_N$	1.6	$6.2 \cdot 10^{-8}$	$1.8 \cdot 10^{-20}$	0.96	87.73
21	$A4B2G2_N$	1.2	$4.1 \cdot 10^{-8}$	$1.9 \cdot 10^{-20}$	1.	102.9
22	$A4B2G3_N$	1.6	$5.1 \cdot 10^{-8}$	$2. \cdot 10^{-20}$	1.	89.31
23	$A4B4G4_N$	0.25	$1.6 \cdot 10^{-8}$	$1.5 \cdot 10^{-20}$	0.99	79.82
24	$A4B4G5_N$	0.84	$3.3 \cdot 10^{-8}$	$1.9 \cdot 10^{-20}$	0.98	64.45
25	$A4B5G4_N$	0.086	$2.7 \cdot 10^{-8}$	$2.6 \cdot 10^{-20}$	0.93	79.03
26	$A4B5G5_N$	1.7	$1.5 \cdot 10^{-10}$	$4.8 \cdot 10^{-20}$	1.	69.08

Zwerger and Müller Newtonian waveforms: i) model name, ii) SNR on AURIGA second run phase 2 expected sensitivity curve for a source at 10 kpc, iii) Total energy radiated in gw, iv) the maximum strain amplitude, v) Fitting Factor with a delta-matched filter and vi) signal duration.

	Model	SNR (10 kpc)	Total Energy ($M_\odot c^2$)	h_{TTmax}	FF	T (ms)
1	$A1B1G1_R$	1.2	$2.1 \cdot 10^{-8}$	$8.4 \cdot 10^{-21}$	1.	109.1
2	$A1B2G1_R$	2.0	$6. \cdot 10^{-8}$	$1.6 \cdot 10^{-20}$	1.	114.0
3	$A1B3G1_R$	2.3	$1.2 \cdot 10^{-10}$	$2.4 \cdot 10^{-20}$	1.	134.0
4	$A1B3G2_R$	1.9	$6. \cdot 10^{-8}$	$1.5 \cdot 10^{-20}$	1.	108.4
5	$A1B3G3_R$	1.5	$1.3 \cdot 10^{-8}$	$5.8 \cdot 10^{-21}$	1.	69.76
6	$A1B3G5_R$	0.44	$3. \cdot 10^{-10}$	$1.1 \cdot 10^{-21}$	1.	57.01
7	$A2B4G1_R$	0.036	$4.5 \cdot 10^{-9}$	$4.9 \cdot 10^{-21}$	0.94	198.8
8	$A3B1G1_R$	2.0	$7.1 \cdot 10^{-8}$	$1.7 \cdot 10^{-20}$	1.	114.9
9	$A3B2G1_R$	2.4	$1.8 \cdot 10^{-10}$	$2.6 \cdot 10^{-20}$	1.	134.2
10	$A3B2G2_R$	2.6	$1. \cdot 10^{-10}$	$1.9 \cdot 10^{-20}$	1.	99.23
11	$A3B2G4_R$	1.2	$8.2 \cdot 10^{-9}$	$4.6 \cdot 10^{-21}$	0.99	59.66
12	$A3B2G4_s$	2.1	$1.2 \cdot 10^{-8}$	$5.5 \cdot 10^{-21}$	1.	59.45
13	$A3B3G1_R$	0.90	$2.1 \cdot 10^{-10}$	$8.7 \cdot 10^{-21}$	0.99	129.3
14	$A3B3G2_R$	1.5	$1.2 \cdot 10^{-10}$	$1.2 \cdot 10^{-20}$	0.98	108.8
15	$A3B3G3_R$	1.7	$5.1 \cdot 10^{-8}$	$1.1 \cdot 10^{-20}$	0.99	79.35
16	$A3B3G5_R$	0.46	$1.9 \cdot 10^{-9}$	$2.3 \cdot 10^{-21}$	1.	58.65
17	$A3B4G2_R$	0.10	$6.1 \cdot 10^{-9}$	$5.3 \cdot 10^{-21}$	0.98	119.1
18	$A3B5G4_R$	0.043	$1.5 \cdot 10^{-9}$	$4.3 \cdot 10^{-21}$	0.95	87.56
19	$A4B1G1_R$	2.5	$1.2 \cdot 10^{-10}$	$2.2 \cdot 10^{-20}$	1.	120.0
20	$A4B1G2_R$	2.9	$1. \cdot 10^{-10}$	$2. \cdot 10^{-20}$	1.	89.12
21	$A4B2G2_R$	4.8	$3.6 \cdot 10^{-10}$	$3. \cdot 10^{-20}$	1.	104.0
22	$A4B2G3_R$	3.5	$2. \cdot 10^{-10}$	$2.2 \cdot 10^{-20}$	1.	89.80
23	$A4B4G4_R$	0.55	$2.3 \cdot 10^{-8}$	$1.1 \cdot 10^{-20}$	0.98	77.28
24	$A4B4G5_R$	0.20	$2.7 \cdot 10^{-8}$	$9.1 \cdot 10^{-21}$	0.97	66.15
25	$A4B5G4_R$	0.16	$2.2 \cdot 10^{-8}$	$1.5 \cdot 10^{-20}$	0.96	77.35
26	$A4B5G5_R$	1.9	$1.4 \cdot 10^{-10}$	$2.1 \cdot 10^{-20}$	1.	66.12

Dimmelmaier, Font and Müller Relativistic waveforms: i) model name, ii) SNR on AURIGA second run phase 2 expected sensitivity curve for a source at 10 kpc, iii) Total energy radiated in gw, iv) the maximum strain amplitude, v) Fitting Factor with a delta-matched filter and vi) signal duration.

2.2 Coalescing Binaries

The coalescence of binary systems (NS-NS, BH-BH and BH-NS) is generally considered as one of the most important sources of gravitational waves [30]: the orbits of the binary system gradually decay through gw emission on a time scale highly dependent on the total mass of the binary system [2]. The entire process is usually divided into three overlapping phases for BH-BH binaries, while NS-NS and BH-NS have only the first two phases:

- an inspiral phase, whose timescale is much longer than the orbital period, giving a chirping signal, with a definite time-frequency relation;
- a merger phase, heavily dependent on the parameters of the collision and therefore very difficult to predict;
- a ringdown phase, characteristic of a deformed BH, whose signal should be a superposition of dumped sinusoids, with *a priori* unknown relative amplitude and phases.

2.2.1 Inspiral

The Inspiral phase can be described as two rotating point particles with intrinsic spins and masses m_1 and m_2, whose orbital parameters evolve secularly due to gravitational radiation. The radiation removes orbital binding energy, which leads to a faster orbiting. This process is adiabatic till the gravitational radiation reaction acts on a timescale which is much longer than the orbital period. The energy spectrum of the inspiral phase is a decreasing function of the frequency f [23],

$$\frac{dE}{df} = \frac{(\pi G)^{2/3}}{3}\mathcal{M}^{5/3} f^{-1/3} \tag{2.2}$$

where $\mathcal{M} = (m_1 m_2)^{3/5} (m_1 + m_2)^{-1/5}$ is the so-called chirp mass.
During the inspiral phase, relativistic effects are large as the orbital velocity gets closer to the speed of light. The gravitational waveform is then determined by the relativistic gravitational interaction between the two point masses and all the other complicated effects (tidal distortion, magnetic fields interaction, etc.) act as small perturbations, allowing an accurate prediction of the waveform. As a consequence, the detection hopes rely mostly on this first phase, while chirping signal achieve

[2] For gravitational radiation to successfully drive the merging phase, the initial orbital period must be $\lesssim 0.3$ days $(M/M_\odot)^{5/8}$, with M the total mass of the system [32]

AURIGA detection bandwidth (close to 1 kHz) in its final phase. The event rate for NS-NS is fairly well known from observations of progenitors in our galaxy and was estimated to be nearly 3 per year in a 200 Mpc volume [39] but, as reported in the introduction, this rate has been recently increased by a factor 6-7 by [3]. The event rates for BH-NS and BH-BH coalescences are far less accurate, but the inspiral waves are expected to be stronger than the NS-NS, due to their greater mass.

2.2.2 Merger

From the adiabatic inspiral in his late evolution, the binary system undergoes a transition to an unstable plunge, induced by strong spacetime curvature: at this point, even if the radiation reaction could be turned off, the companions would still merge. The plunge and the collision are generally called merger phase. Unfortunately, this phase (either for NS-NS or NS-BH) is still poorly understood, resulting in a lack of reliable waveforms and energy spectra.

2.2.3 Ringdown

As the final BH is settling down to a stationary Kerr state, it should undergo damped vibrations, which can be seen as oscillations of the final BH quasi-normal modes. The most slowly damped mode, which has spherical harmonic indices $l = m = 2$, dominates over the other modes at late times. Focusing on this last Quasi-Normal Ringdown (QNR) mode, the energy spectrum is just a resonance curve [40],

$$\frac{dE}{df} = \frac{A^2 M^2 f^2}{32\pi^3 \tau^2} \left\{ \frac{1}{\left[\left(f - f_{QNR}\right)^2 + \left(2\pi\tau\right)^{-2} \right]^2} + \frac{1}{\left[\left(f + f_{QNR}\right)^2 + \left(2\pi\tau\right)^{-2} \right]^2} \right\}, \tag{2.3}$$

peaked at f_{QNR} with a width given by the inverse of the damping time,

$$\Delta f \sim \frac{1}{\tau} = \frac{\pi f_{QNR}}{Q\left(a\right)},$$

where the quality factor of the mode Q is given by

$$Q\left(a\right) = 2\left(1 - a\right)^{-\frac{9}{20}}$$

A is a dimensionless coefficient that describes the magnitude of the perturbation when the ringdown begins, M is the mass of the BH and a is the spin of the final

BH. The value of the spin depends on the initial parameters of the system, which are difficult to predict, nevertheless, since the BH may typically have spun up to near maximum rotation, we can assume $a = 0.98$ [32]; the resonance frequency and the quality factor are then:

$$\begin{cases} f_{QNR} = \frac{0.13}{M} \\ Q \simeq 12 \end{cases}$$

For a BH mass $M = (28 \div 31) M_{\odot}$ the signal spectrum is substantially coincident with the AURIGA second run detection bandwidth.

2.3 Gamma-ray Burst Models

Gamma-Ray Bursts are the most luminous events in the Universe. Current models explain the origin of "long" GRB ($t_{\gamma} \gtrsim 2$ s) [44] in the coalescence of a NS and a rotating BH, where the latter may form a matter torus surrounding the BH [37]; other models call for a class of massive supernovae collapsing to form a spinning BH. Although the association between GRB and star collapse (Hypernovae or Collapsars stars) is sure for at least a few GRBs, the BH-Torus models are very interesting because: i) they are excellent candidates for the ultimate energy source of GRB ($\sim 10^{53}$ erg) and ii) they are expected to emit gravitational waves [34], [35].
In particular, this last model, a $1.4 M_{\odot}$ NS and a $7 M_{\odot}$ BH binary system evolves towards a torus through the disruption of the NS, surrounding the BH in a suspended accretion state, which should last several seconds ($10 \div 80$ s) before the final collapse. A strong emission of gw occurs, once the torus is formed, due to the lumpiness of the neutronized matter: estimates on the energy released in gw equal the order of magnitude of "traditional" electromagnetic channels. The distinctive characteristics of the above model is a slowly varying frequency and an almost constant amplitude for the emission of gw, also known as the linear chirp.

Compact binary mergers, such as NS-NS, might also be emitters of "short" GRBs [45]: this could be interesting from the point of view of gw research, since these systems, as reported in the previous paragraph, are strong gw emitters. However, binary mergers have natural channels of emission along their rotational axis and they may therefore produce beamed GRBs: current afterglows observations, though, indicate that only "long" GRBs are beamed, with opening angles of a few to tenths of degrees. There is no such evidence for "short" GRBs.
As a matter of fact, for all these models the amplitude of gw strain is expected

to be $h \sim 10^{-23} \div 10^{-21}$ at cosmological distances, i.e. $1 \div 3$ orders of magnitude below the sensitivity of present and planned ground-based gw detectors.

Chapter 3

Single detector estimation methods

A gw impinging transversally to the bar axis deposits energy in the first compression mode of oscillation. To detect this tiny signal, an auxiliary oscillator is attached to one of the bar faces and its resonance frequency is tuned to that of the bar sensitive mode, in order to have a strong coupling. This transducer is in turn electrically coupled to the external readout. Many different solutions have been tested: capacitive, inductive, microwave and optical. The raw data at the output of the readout system are the starting point of the data analysis.

We now assume that we observe, in the presence of noise, a burst whose characteristics are known except a few parameters. In our study, we have focused on short (duration $\leq$ 100 ms) bursts, whose spectral density is ranging over the designed bandwidth of AURIGA in its ultra-cryogenic configuration (Phase 2; see figure 1.4), and obviously, with sufficient strain amplitude to be observed over the expected detector noise.

Two pipelines corresponding to different approaches to the signal detection have been recalled: a template search based on the matched filter, under the hypothesis of a complete *a priori* knowledge of the signal waveform; a *blind* search based on the Excess Power method, which makes minimal assumptions (i.e. the duration) on the unknown gw burst.

For the template search, assuming a signal embedded in addictive gaussian noise, we can resort to the Maximum Likelihood theory to estimate signal parameters. This "near-optimal" data analysis, is able to recognize gw signals and extract the signal parameters without distortion of their probability distributions [62].

The burst parameters, the amplitude A and Time Of Arrival TOA, are determined

by matched filtering. At low SNRs, there is a large ambiguity in their estimation: this uncertainty makes genuine burst gravitational wave signals almost indistinguishable from events arising from un-modelled environmental noise sources. In fact, the χ^2 -test does not have enough statistical power to identify the signal template and/or parameters in the low SNR regime.
The Excess Power search is less restrictive with respect to the signal waveform but, compared to the previous method, requires higher selection thresholds to get rid of the increased number of FA.

3.1 The AURIGA Matched Filter

If we suppose that the overall system (the bar, the transducer and the double dc squid amplifier) is linear and time-invariant and, in addiction, that gaussian stationary noise is superimposed to the signal, then the matched filter is the minimum-variance unbiased linear estimator of the signal amplitude. In our case, such filter is usually matched to a delta function, the so called (Wiener-Kolmogorov Filter, WK) [1] and is applied continuously to the data of the AURIGA detector.
The identification of candidate events is performed in the time domain, by a max-hold algorithm. This algorithm identifies the time and the amplitude of the extremes of the filtered data separated by at least a time span about 3 times the reciprocal of the effective bandwidth of the system (i.e. ~ 0.1 second for a 80 Hz bandwidth).
An adaptive threshold [2] is then applied to select candidate events for further investigations. Finally, to increase the timing resolution below the sampling time, we have adopted an algorithm of interpolation [61] to estimate the event amplitude and time of arrival.
Our standard estimation method is then the result of : i) the adaptive WK filter, ii) the max-hold algorithm + the adaptive threshold, as candidate event selection method and iii) the interpolation algorithm to calculate the event parameters, A and TOA, with greater accuracy.
There are two reasons to establish a threshold on candidate events:

1. the trigger search algorithm has strong biases in amplitude and arrival time at least up to SNR$= 4 \div 5$. The bias is in this case due to the fact that we

[1] In the new AURIGA data analysis, a thorough work has been done in these last months to implement the possibility to filter for any arbitrary waveform.

[2] for example, during the first run of AURIGA, a $\mathrm{SNR_{thr}} = 5$ was applied to produce the list of candidate events for coincidence analysis with the other gw detectors.

cannot know the true time of arrival of the gw signal; the max-hold algorithm looks for the nearest large fluctuation of the noise and the trigger cannot be related with the injected waveform;

2. for SNR> 5 the False Alarms rate (FAr) falls down to acceptable levels for gw detections [66]. As the SNR grows up, there is less chance for a noise fluctuation to reach such a SNR level and the max-hold locks to the real trigger. In this case, the estimated amplitude becomes unbiased and the time of arrival error strongly peaks around zero.

It should be noticed that the bias in TOA is unavoidable as the arrival time estimate is a non linear algorithm, which can be linearized at high SNR around the true arrival time [48].

To cope with the problem of biases in the signal estimation, we can resort to the maximum likelihood criterion; it is equivalent, in the presence of gaussian noise, to the standard Wiener filtering together with the χ^2 test of the goodness of the fit [62]. The χ^2 value (which is statistically independent of the amplitude for signals which pass the test) can be used to test the consistency of our *a priori* hypothesis on the signal template.

3.1.1 Timing errors, bias on the SNR and ROCs

In the time domain, the signal after the WK filter appears as a damped beat between the system modes, modulating a sinusoidal carrier wave [61]. In the new hardware configuration, the two modes are more separate; hence, near the TOA the relative amplitudes of the peaks decrease faster than what happened for the previous AURIGA (the beat modulation is of the same order of the exponential decay): this allows for an improved timing accuracy. In the low SNR regime, the TOA is expected to be a zero-mean random variable with a distribution made of multiple gaussian peaks; these peaks are spaced by the half-period of oscillation of the antenna and have gaussian distributed relative amplitudes, as shown by figure 3.1, for a MonteCarlo simulation of N=3647 delta-like bursts at SNR=10.

We split the timing error Δt_{err}, in the sum of *phase* error Δt_ϕ, and *peak* peak number k multiplied by the period $T = 2\pi/\omega_0$ of the carrier wave:

$$\Delta t_{err} = \Delta t_\phi + k \cdot T, \tag{3.1}$$

If we look for an asymptotic solution, for large SNR, it can be demonstrated [61]

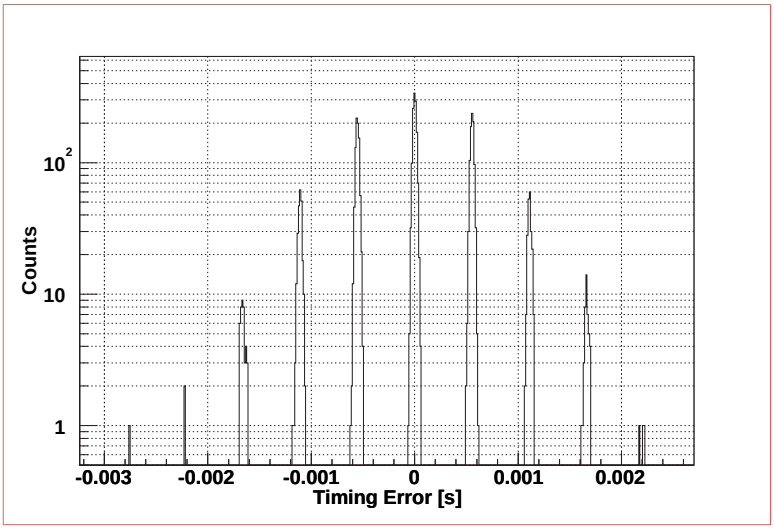

Figure 3.1: Timing Error distribution for delta-like bursts at SNR= 10 (N=3647 trials). The distribution has a small bias ($\sim 3\mu s$), while the overall rms of all the peaks is $615\mu s$.

that the standard deviation of the errors is equal to:

$$\sigma_{t\phi} = \frac{1}{\omega_0 \mathrm{SNR}}, \tag{3.2}$$

and

$$\sigma_{\mathbf{k}} = \frac{\omega_0}{\pi \omega_* \mathrm{SNR}}. \tag{3.3}$$

Equation 3.11 is the classical formula for the *phase* timing of narrow band signals leading to the well-known Cramèr-Rao Lower Bound (CRLB), which will be briefly introduced in paragraph 3.4.1.

In figure 3.2, we show the timing error as a function of the injected SNR:

- the upper points (yellow) refer to the standard deviation of the errors on the TOA (N=35977 trials each SNR); the error bars are conservative and are computed according to 95% probability of FD by setting $k = 4.2$ through the Bienaymè-Tchebyscheff inequality [3]

[3]The FD probability is upper bounded by:

$$FD \leqslant P\left\{\Delta t_{err} \geqslant k\sigma^2_{terr}\right\} \leqslant \frac{1}{k^2} \equiv P_T. \tag{3.4}$$

where P_T is the maximum FD probability computed through the Bienaymè-Tchebyscheff inequality.

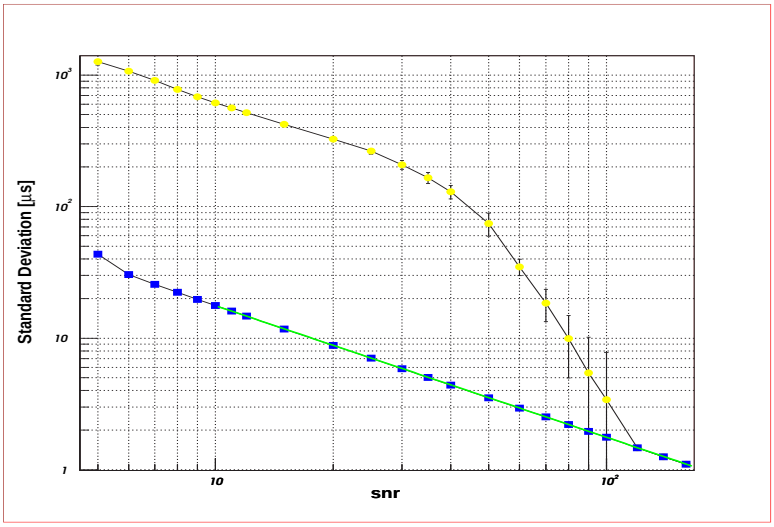

Figure 3.2: Timing Error vs SNR: Δt_{err} (yellow) and Δt_{ϕ} (blue) as a function of the SNR.

- lower points (blue) refer to the standard deviation of the phase error; $\sigma_{t\phi}$ matches perfectly the theoretical curve given by the CRLB (in eq. 3.11), $f(x) = P_0/x$; the fitting value $P_0 = (176.6 \pm 0.9)$ μs is the inverse of the central frequency $\omega_0 = 5661$ rad/s calculated from the parameters in table 1.2.

At SNR=11, $\sigma_k < 1$ and $\sim 70\%$ of injected signals are in the central peak and, as shown, for SNR$> 80 \div 90$, Δt_{err} collapses to the CRLB (within conservative errors). At low SNRs, in the ambiguity region, the WWLB (see following paragraph 3.4.2) gives a tighter lower bound on time estimates for a wide range of SNRs [60].

As it concerns the SNR estimation, we have performed a Montecarlo simulation: first, by injecting δ signals (N=35981 trials for each tested SNR) in 10 hours of simulated data and then by estimating the amplitude of the resulting events. Figure 3.3 shows the histograms for $\mathrm{SNR}_0 = 1$ (red), 2 (violet), 8 (blue). At low SNR, the estimation method is no more linear and a large bias towards greater amplitudes appears. The expected SNR biases are, respectively: $\Delta\mathrm{SNR}(1) = 1.952 \pm 0.003$, $\Delta\mathrm{SNR}(2) = 1.284 \pm 0.007$ and $\Delta\mathrm{SNR}(8) = 0.123 \pm 0.005$. The ensemble of the WK filter, the max-hold algorithm, a determined threshold, and the interpolation algorithm is called the Standard Estimation Method (SEM). The results obtained with this model, implemented in AURIGA data analysis, provide unbiased (i.e. $\Delta\mathrm{SNR}/\mathrm{SNR} \leq 0.1$) amplitudes for signals with SNR≥ 5.

Finally, we report the Receiver Operating Characteristics (ROC) curves (see

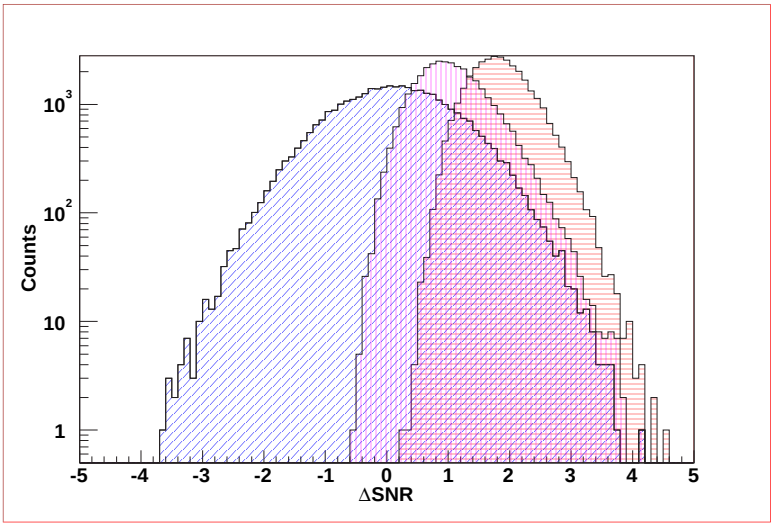

Figure 3.3: Montecarlo of N=35981 trials : the histograms of the estimated SNRs (diminished by the true SNR_0, $\Delta\mathrm{SNR} = \mathrm{SNR} - \mathrm{SNR}_0$) for injected signals at $\mathrm{SNR}_0 = 1$ (red), 2 (violet), 8 (blue). For the first two case, the estimation method is no more linear and a bias toward greater amplitudes appears. In the last case, instead, the histogram reproduces the zero-mean Normal density function of the underlying stochastic process, as predicted by linear estimation theory. Note that this happens already at SNR=5, but, for graphical reasons, we have chosen not to show it.

appendix A) for the SEM.
These curves, shown on figure 3.4, allow a quick comparison among different algorithms: they display the detection efficiency (for injected delta-like signals of different amplitude) versus the FAr. As the key parameter for this method is the threshold [4], we have estimated acceptance as a function of the threshold itself on a population of $N = 35997$ injected signals for SNR=5,6,7. These are the lowest SNRs which can be taken in consideration neglecting the bias on the amplitude and on the time of arrival.

The FArs shown on figure 3.4 refer to gaussian stationary noise and are estimated analytically by means of a conservative upper limit: in fact, it would take thousands of years of data to calculate the leftmost points on the graph. As a matter of fact, it is well known that the main problem in real data comes from spurious events (environmental noises) and that these outliers are much more fre-

[4]Note that it is easy to put up different decision algorithms, which do not depend on a threshold: for example, instead of selecting candidate events on threshold-crossing, one can choose the M largest events in each day. In such case, the key parameter would be M and the FAr on the single detector would be fixed once for all.

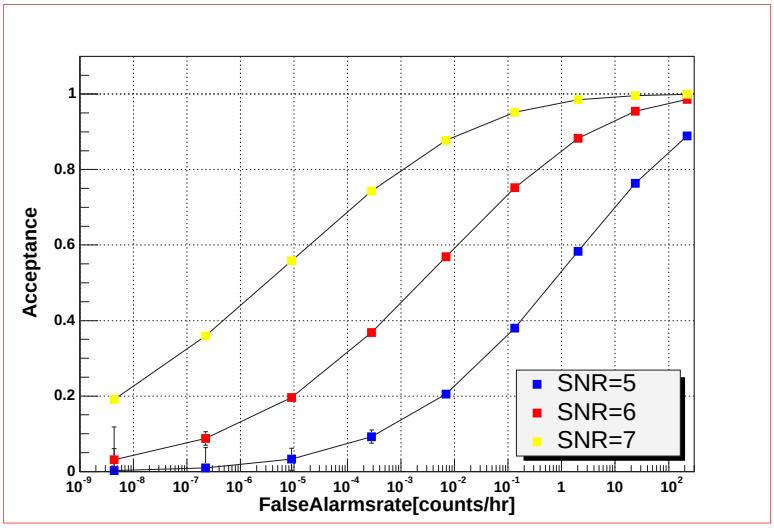

Figure 3.4: ROC curves for the SEM (SNR=5,6,7). Once having fixed a tolerable FAr (depending strictly on the purpose of the analysis: for example, the accepted FAr for detectors participating the Supernova Watch Search is one every 100 years), the comparison with other algorithms is on the detection efficiency.

quent (at higher thresholds) than the expected FAr of gaussian stationary noise. Nevertheless, the key point is to keep under control the events arising from noise fluctuations. To get rid of spurious signals, it is necessary to perform a multi-detector analysis.

3.2 Maximum Likelihood Estimators of Signal Parameters

Let us assume that the sampled data stream of a gw detector is given by the superposition of a deterministic function $f(t)$ (the signal) and a stationary gaussian stochastic process $\eta(t)$ (the noise):

$$x_i = \eta(t_i) + Af(t_i - t_0, \vartheta) \ , \tag{3.5}$$

where $t_i = i\Delta t$, with Δt the sampling time and i an integer index, $\eta(t_i)$ has zero mean and correlation $\langle \eta(t_i)\eta(t_i) \rangle = \sigma_{ij}$ ($\langle \dots \rangle$ means ensemble average) and $f(t, \vartheta)$ is a known function of time and of the parameter set ϑ.

In order to extract the value of the signal amplitude, A, the TOA t_0 and the other parameters ϑ, the Maximum Likelihood procedure searches the parameter

values that maximize the probability of occurrence of the observed data set, or equivalently, that correspond to the minimum of the negative of logarithmic likelihood $\Lambda(A, t_0, \vartheta)$:

$$\Lambda(A, t_0, \vartheta) = \frac{1}{2} \sum_{i,j=1}^{N} \mu_{ij}[x_i - Af(t_i - t_0, \vartheta)][x_j - Af(t_j - t_0, \vartheta)] \ , \tag{3.6}$$

where μ_{ij} is the inverse of the correlation matrix σ_{ij}.

For given values of t_0 and ϑ the minimum of $\Lambda(A, t_0, \vartheta)$ as a function of A is found analytically at

$$A_{opt}(t_0, \vartheta) = \frac{\sum_{i,j=1}^{N} \mu_{ij} x_i f(t_j - t_0, \vartheta)}{\sum_{i,j=1}^{N} \mu_{ij} f(t_i - t_0, \vartheta) f(t_j - t_0, \vartheta)} \ , \tag{3.7}$$

and it amounts to:

$$\Lambda_{min}(t_0, \vartheta) = \frac{1}{2} \sum_{i,j=1}^{N} \mu_{ij} x_i x_j - \frac{A_{opt}^2(t_0, \vartheta)}{\sigma_A^2} \ . \tag{3.8}$$

The square of the uncertainty on $A_{opt}(t_0, \vartheta)$ turns out to be

$$\sigma_A^2 = \frac{1}{\sum_{i,j=1}^{N} \mu_{ij} f(t_i - t_0, \vartheta) f(t_j - t_0, \vartheta)} \ . \tag{3.9}$$

The linear combination of the data in eq. 3.7 is just the discrete Wiener optimal filter matched to the function $f(t)$. On the other hand, eq. 3.8 shows that, in order to minimize $\Lambda(A, t_0, \vartheta)$ as a function of the TOA, t_0, and ϑ, one has to maximize the square of the signal to noise ratio. This means that once one has set up the Wiener filter for the data, the best estimate of the parameters is the one that maximize the filter output. As usually the dependence of σ_A on t_0 and ϑ is very weak, this just implies that one has to maximize $A_{opt}(t_0)$. The minimum value of $2\Lambda(A, t_0, \vartheta)$ has to be distributed as a χ^2 with $N - N_\vartheta - 2$ degrees of freedom, with N_ϑ the number of elements of the parameter set ϑ.

3.3 Excess Power through Karhunen-Loève Expansion

Though some of the candidates sources, like coalescing binaries in the initial phase of spiralling, have been modelled with great accuracy, allowing the construction of

trustful gw templates, and hence the implementation of matched filter, it is clear that the uncertainty on the burst waveforms of the great part of the gw possible sources (like supernova core collapses or merging phases of a binary system) is still long to go. Moreover, the available waveforms highly depend on some set of arbitrarily chosen parameters through the result of some simulation.

We note that for narrow band detectors (such as AURIGA during his first scientific run), the simplified hypothesis of a $\delta - like$ incoming signal (i.e. with a flat response over the detector bandwidth), even though somehow restrictive, was a reasonably good approximation, since the two resonant modes were only $\sim 20Hz$ far apart. With the present AURIGA bandwidth ($\sim 70Hz$), such hypothesis is even more restrictive with respect to all possible incoming gw waveforms.

In such context, a realistic detection strategy have to cope with poorly modelled, or not modelled at all, gw signals.

This problem has already been faced from different point of views:

- Much work has been devoted by the LIGO group to implement and test new "blind" strategies (the so-called Event Trigger Generators ETG): TFclusters [52], Excess Power [53], [54], WaveBurst [56]. These ETGs are currently used in data-analysis of latest LIGO science runs.

- Within the Virgo group, some authors devised several simple algorithms (i.e. the Norm filter, the mean filter, the Slope filter, the ALF and the Peak Correlator) to be run in parallel [55]; A. Vicerè [49] has proposed a kind of Excess Power Search based on the Karhunen-Loève Expansion, KLE (see Appendix B for a brief introduction on the subject). These procedures need a thorough test and optimization against model waveforms [51], [50].

Following a previous internal work [57] and with a careful look at the most recent papers on Excess Power [54], [49], an Excess Power method based on the KLE has been recently implemented in AURIGA data-analysis. It consists of two main steps:

- we apply the WK filter (δ-matched filter) to the detector output;

- we then perform an Excess Power search on a test statistic similar to the energy, which can be easily calculated by means of the KLE.

Such approach looks very promising, even though it still lacks an exhaustive bench-testing.

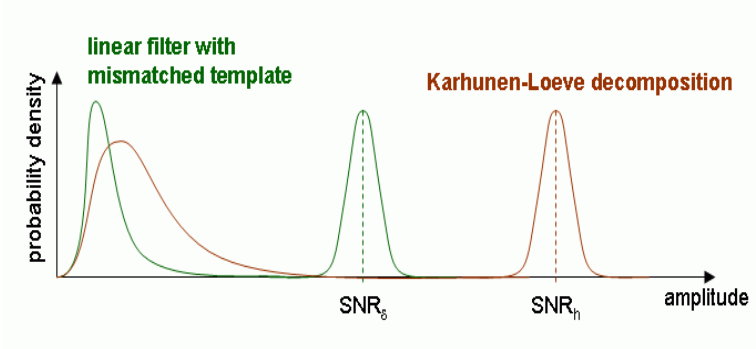

Figure 3.5: SNR distributions ($\mathcal{H}_0$ and $\mathcal{H}_1$) for a mismatched linear filter (green) and for the KLE (red).

For any waveform, this method allows for the recovery of all the in-band signal spectral energy with the sole assumption of knowing *a priori* the signal duration, T_{KL}: the SNR through KLE equals the maximum one achievable by means of a filter matched to the signal, under the hypothesis of waveform complete knowledge. The drawback is the increased tail of fake events at a given threshold. A typical comparison between SNR distributions of a mismatched filter (e.g. WK filter) and of the KLE of an unknown signal $h(t)$ is depicted on figure 3.5: it is possible to note that: i) the KLE (red line) recovers the correct SNR_h, but the distribution of noise events follows a χ distribution (the T_{KL} fixes the degrees of freedom); ii)for the WK filter (green line), the SNR_δ is smaller due to the filter mismatch, but the tail of noise events follows the gaussian statistic.

3.3.1 Statistical analysis

Let us write the detector output signal $x(t)$ as a vector of samples at the instance $t_i = \frac{i}{N}T$, with $i = 1, ..., N$. Let $\mathbf{x} = (x_1, \ldots, x_N) = (x_{t_1}, \ldots, x_{t_N})$ be such data vector. This vector can be written as the sum of signal and noise coefficients of the KLE, respectively h_k and n_k:

$$\mathbf{x}_k = \sum_k^N (h_k + n_k)\, \psi_k. \tag{3.10}$$

ψ_k being the $k-$th eigenvector of the correlation matrix $\mathbf{R}^{-1}$ (see Appendix B), and therefore through the equation B.2 the δ-filtered data $\mathbf{f}_\delta$:

$$\mathbf{f}_\delta = \mathbf{R}^{-1}\mathbf{x} = \sum_k^N \frac{1}{\sigma_k^2}\,(h_k + n_k)\,\psi_k, \tag{3.11}$$

where σ_k are the correlation matrix eigenvalues. Consider test statistic L,

$$L = \mathbf{f}_\delta^T \cdot \mathbf{R}\mathbf{f}_\delta = \sum_k^N \frac{1}{\sigma_k^2}\,(h_k + n_k)^2, \tag{3.12}$$

this expression, which is similar to the power $(f_\delta \cdot f_\delta)$, is the optimal statistic for an unknown burst with a flat prior [49]. The sole reason for applying the KLE is that it allows for more flexibility in the calculation of L: in particular, we can decide, for instance, that some of the basis elements correspond to large noise components and, therefore, that such components can be omitted without loosing significant fractions of SNR. Due to the fact that the coefficients of the KLE are uncorrelated, this procedure corresponds to simply restricting the summation over a number $N_\parallel$ of eigenfunction such that $N_\parallel \leq N$.

The distribution of the statistic L is a χ^2 with $N(N_\parallel)$ degrees of freedom under the hypothesis $\mathcal{H}_0$ (no signal); in case of $\mathcal{H}_1$ (signal of unknown shape, h) the L is distributed as a non-central χ^2 with $N(N_\parallel)$ degrees of freedom and the square of the optimal filter signal-to-noise ratio SNR^2 as non-central parameter.

3.3.2 Timing errors and bias on SNR

In this paragraph, we briefly describe preliminary results of the Excess Power search implemented in AURIGA data analysis.

The TOA is assumed to have a uniform *a priori* distribution over the interval $[0,T_{KL}]$; to estimate it, we have devised a Minimum Mean Square Error (MMSE) algorithm:

$$t_{MMSE} = \frac{\sum_k^N kT_s e^{\frac{\mathbf{R}(kT_s)}{f\sigma_N^2}}}{\sum_k^N e^{\frac{\mathbf{R}(kT_s)}{f\sigma_N^2}}}, \tag{3.13}$$

where T_s is the sampling time, $\mathbf{R}$ is the correlation matrix, σ_N is the standard deviation of the N samples and f is a free parameter to be tuned.
Testing this estimator, it turned out that the optimal value for f is weakly related to the SNR of simulated signals and to the T_{KL} fixed for the search: over a wide range of SNR ($5 \div 160$) and of T_{KL} (10 ms $\div$ 50 ms). The choice of $f = 0.3$ produces

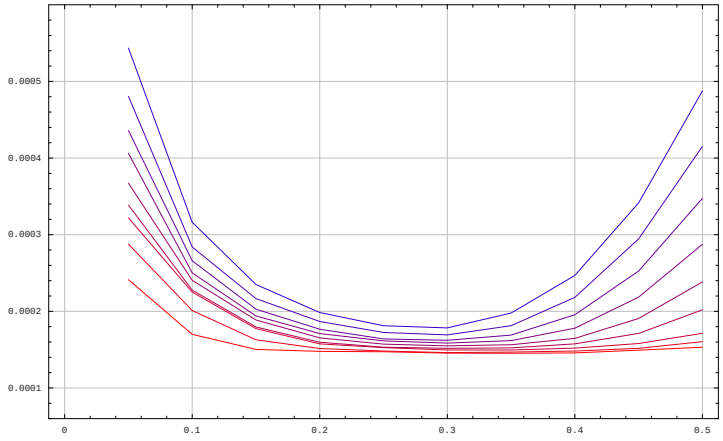

Figure 3.6: The σ_{terr} vs. f as a function of the T_{KL} for SNR=50

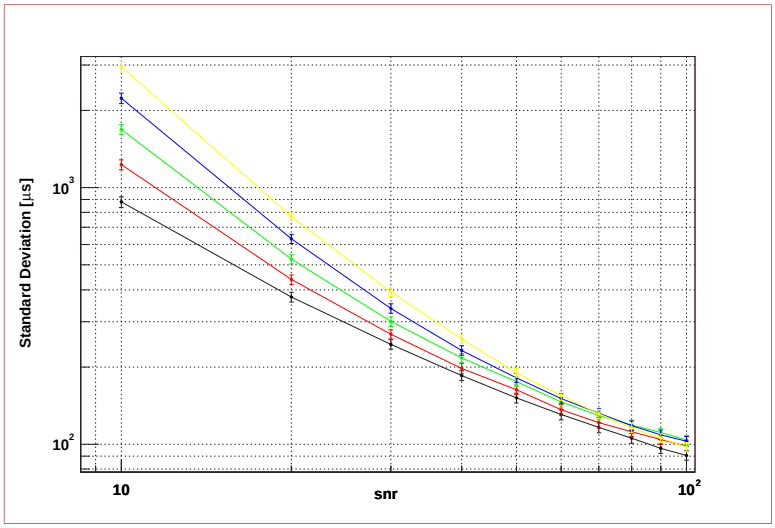

Figure 3.7: The bias on the estimated SNR vs. SNR as a function of the T_{KL} (10 ms (black), 20 ms (red), 30 ms (green), 40 ms (blue) and 50 ms (yellow)).

timing errors which are less than 10% larger than the minimum attainable ones (see figure 3.6).

As a preliminary result, we show the timing errors as a function of SNR for a set of simulations with N=35997 injected δ-like signals on figure 3.7 and the bias on the estimated SNR as a function of the SNR itself for the same set of simulations on figure 3.8.

As regards the ROC curves for the Excess Power method, it is straightforward to find a template for which this method is favorable to the WK filter: as the KLE

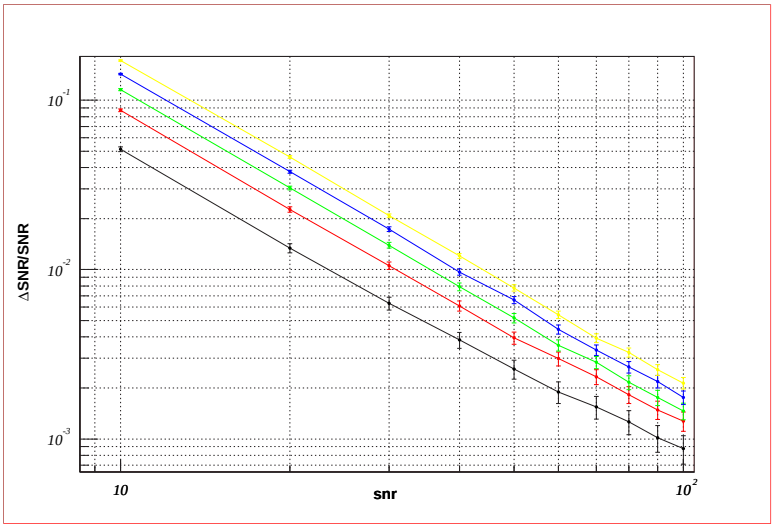

Figure 3.8: The σ_{terr} vs. SNR as a function of the T_{KL} (10 ms (black), 20 ms (red), 30 ms (green), 40 ms (blue) and 50 ms (yellow)).

eigenvectors are a complete basis in the vector space of all possible data vectors of dimension N, any of such eigenvectors (except the one representing the δ function) is orthogonal to the δ. Almost all of the SNR is lost by the WK filter because of this mismatch. By the way, those templates have currently no correspondence in the astrophysical models, which, on the frequency scale of the AURIGA bandwidth ($\sim 80 \div 100$ Hz), show no great deviations from a flat spectrum: at least, these deviations do not affect the detection probability of the WK filter in such a way to counterbalance the longer tail of FA produced by the Excess Power. This method too calls for a multi-detector data analysis to cut all fake events.

3.4 Error Bounds

To investigate the performances of a specific estimator, it is useful to resort to the well known and widely used lower bounds on the Mean Square Error (MSE). The most commonly used bounds include the Cramèr-Rao Lower Bound (CRLB) and the Weiss-Weistein Lower Bound (WWLB).

3.4.1 Cramèr-Rao Lower Bound

The CRLB treats the unknown parameter, θ, as a deterministic quantity and provide bounds on the MSE in estimating any selected value of the parameter: for

this reason it is often referred to as a *local* bound.

Consider a waveform characterized by a set of parameters, A, t_0 and ϑ (for the sake of simplicity we shall refer to the ensemble of parameters as the parameter vector θ), which is superimposed to additive gaussian noise (just like in equation 3.5): the CRLB affirms that the error covariance matrix of any parameter vector $\widehat{\theta}$, evaluated by means of an *unbiased* estimator, is always larger than or equal to the inverse of the Fisher information $\mathcal{I}$ at θ:

$$\mathcal{R}_{ij} = \left\langle \left(\hat{\theta}_{\mathbf{i}} - \theta_{\mathbf{i}}\right)\left(\hat{\theta}_{\mathbf{j}} - \theta_{\mathbf{j}}\right)\right\rangle \geq \mathcal{I}_{ij}^{-1}, \tag{3.14}$$

where the elements of $\mathcal{I}_{ij}$ are calculated by [48]:

$$\mathcal{I}_{ij} = \left\langle \frac{\partial^2}{\partial\theta_{\mathbf{i}}\partial\theta_{\mathbf{j}}}\left(\Lambda\left(\mathbf{x}|\theta\right) - \Lambda\left(\mathbf{x}|0\right)\right)\right\rangle, \tag{3.15}$$

and $\Lambda(\mathbf{x}|\theta)$ is the logarithmic likelihood introduced in equation 3.6.

Provided that some general conditions are fulfilled, the CRLB can be written as [48]:

$$\sigma_{\hat{\theta}}^2 \geq \frac{1}{\omega_0^2 \mathrm{SNR}^2 + C/\sigma^2}, \tag{3.16}$$

where C is a constant depending only on the shape of $\hat{\theta}$ distribution, σ is the standard deviation of $\mathbf{x}$ and ω_0 is the so-called Gabor bandwidth (or the rms bandwidth) of the signal f :

$$\omega_0^2 = \frac{\int \omega^2 \left|f\left(\omega\right)\right|^2 d\omega}{\int \left|f\left(\omega\right)\right|^2 d\omega}. \tag{3.17}$$

Though the CRLB is generally the easiest to be evaluated, it does not characterize performances outside the asymptotic region, where estimators are unbiased and, as other *local* bounds, it does not consider any *a priori* information about the parameter space. Further more, it does not take into account the well-known "threshold effect" of time estimators, which is present in narrowband systems [59]. In fact, for SNR below a certain threshold, the MSE increases rapidly as the SNR decreases: in this region, the MSE exceeds the CRLB, mainly due to the peak ambiguity error.

These limitations are clearly visible on figures 3.1 and 3.2. Only if the gw signal is well above the background noise, an independent estimation of A and TOA is then allowed. In such case, the Fisher information matrix provides bounds on the variance of unbiased estimators via the CRLB, but theoretical extension of this

local bound to biased estimators is not trivial [58]. As a consequence, we can resort to a different kind of lower bounds: the Bayesian bounds.

3.4.2 Weiss-Weistein Lower Bound

The Weiss-Weinstein Lower Bound (WWLB) is a Bayesian bound which assume that the parameter is a random variable with known *a priori* distribution. There is no restriction on the class of estimators to which they apply (i.e. like for CRLB) and they can easily incorporate any prior information about parameters to be estimated.

By assuming that the parameter θ represents the time of arrival to be estimated and that it is uniformly distributed in an interval $0 \leq \theta \leq D$, the WWLB can be written as [60]:

$$\sigma_{\hat{\theta}}^2 \geq \max_{0 \leq \theta \leq D} J(h), \tag{3.18}$$

where

$$J(\theta) = \begin{cases} \dfrac{\frac{1}{2}\theta^2\left(1-\frac{\theta}{D}\right)^2 e^{-\frac{\mathrm{SNR}}{2}[1-\mathbf{R}(\theta)]}}{1-\frac{\theta}{D}-\left(1-\frac{2\theta}{D}\right)e^{-\frac{\mathrm{SNR}}{4}[1-\mathbf{R}(2\theta)]}}, & 0 \leq \theta \leq \frac{D}{2} \\ \\ \frac{1}{2}\theta^2\left(1-\frac{\theta}{D}\right)e^{-\frac{\mathrm{SNR}}{2}[1-\mathbf{R}(\theta)]}, & \frac{D}{2} \leq \theta \leq D \end{cases} \tag{3.19}$$

and where $\mathbf{R}$ is the normalized signal autocorrelation function. Note that the WWLB takes into account the peak ambiguity and, except for the SNR, it depends only on the *a priori* known interval D and the autocorrelation function.

Chapter 4

Methods of gw network data analysis

There are many reasons to combine data from geographically separated detectors:

- a better sensitivity with respect to a single detector, since the network noise behaves as almost "isotropic", while gravitational signals are directional;
- higher levels of confidence in the detection and characterization of a signal;
- spurious background reduction;
- the possibility to estimate the direction of arrival and polarization of the incoming gravitational wave.

Ideally, under the hypothesis of knowing the gw waveform in advance, one would apply an optimal filter on the output from a single detector and apply the χ^2-test on the filtered output. However, given current astrophysical predictions and gravitational wave detector sensitivity curves, one expects the signal-to-noise ratios (SNRs) and rates of burst gravitational waves to be very low. At low SNRs (for instance SNR$<$ 15 for the AURIGA first run), there is a large ambiguity in the estimation of the burst parameters, namely arrival time and amplitude [61]. This uncertainty makes genuine burst gravitational wave signals almost indistinguishable from events arising from unknown environmental noise sources. In fact, the χ^2-test does not have enough statistical power to identify the signal parameters in the low SNR regime, as previously shown for resonant-mass detectors by Baggio *et al.* [62]. Thus, to make a distinction between signals and noise, one must cross-correlate data from multiple detectors to reduce contributions from spurious

environmental noise and to increase the SNR of gravitational wave bursts. Hence, methods for performing multi-detector burst searches and the choice of data exchange parameters are crucial for the burst gravitational wave search pipeline.

Burst gravitational wave searches on data from multiple, widely-spaced detectors have already been performed [63], [64]. These searches have put upper-limits to the rates and amplitudes of burst gravitational waves impinging on the earth. An example is the International Gravitational Event Collaboration (IGEC), which developed a framework composed of data format and analysis tools that allowed a thorough analysis of the triggers from the burst search pipeline of 5 resonant-mass detectors [65] [66]. Though this framework allows for a statistically robust analysis, it is currently restricted to the analysis of triggers from resonant-mass detectors.

Astone and Schutz [67] have discussed the idea of narrowbanding interferometers for the purpose of performing a burst search between interferometers and resonant-mass detectors. The drawback to this method is that narrowbanding reduces the sensitivity of the intereferometers to burst signals, but it could be useful for those astrophysical templates (e.g. Quasi-Normal ringdown of perturbed Black-Holes) whose spectral power is concentrated within a narrow band.

In this chapter, we describe briefly four methods for performing burst searches between interferometers and resonant-mass detectors. The first method is a coincidence search and is an extension of the IGEC framework to include the parameters from interferometer burst search algorithms (also known as Event Trigger Generators or ETGs). The second method is the externally triggered search method previously proposed by Finn, Romano and Mohanty [68]. The third method is a consistency method based on the r-statistic of the cross-correlation of two detectors. The fourth method is what we call a "Coherent Network Search" and it has been split in two subsections: the template-based search and the templateless (or "blind") search. In figure 4.1, we show a block scheme of the various possibilities.

4.1 Coincident trigger search

The most straightforward approach to a burst gravitational wave search is to look for coincident excitations between faraway detectors. For such an analysis, candidate burst event lists are independently generated for each detector with a threshold that extract the larger SNR excitations. A search for coincident arrival times is then performed. In addition to correlating the event arrival times, one may also apply additional constraints on other signal parameters such as the amplitude or the orientation of the detector with respect to a fixed direction in the sky for non

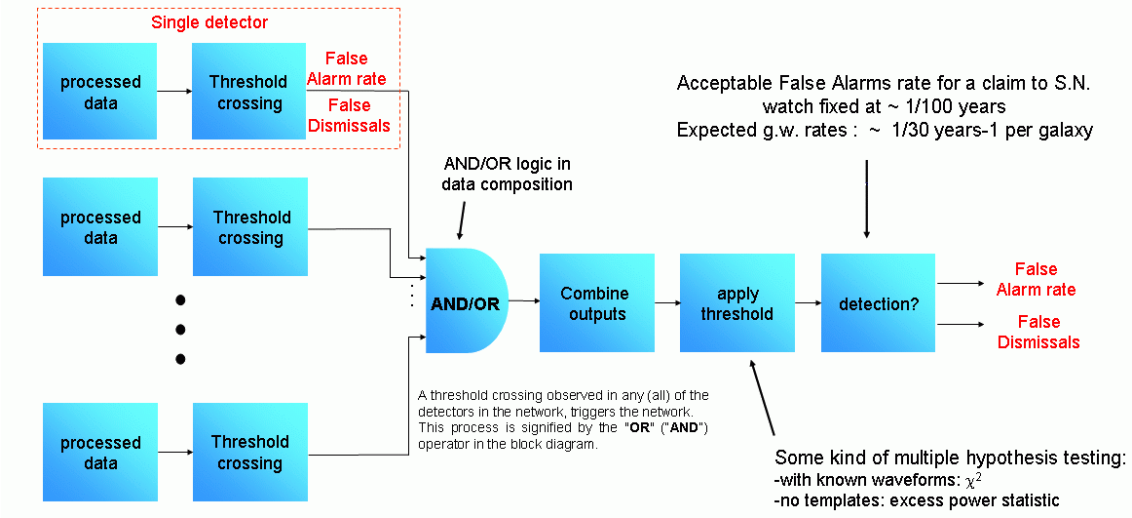

Figure 4.1: Block scheme of a network analysis.

isotropic source distribution, e.g. Galactic sources.

This analysis has been used in several searches in the past and recently by the IGEC [63] [64] [65], [66]. The IGEC has established a complete framework for exchanging data in view of performing a coincidence search. Under this framework, it is mandatory to exchange the time of occurrence, amplitude and duration of a trigger and the time spans of detector operation [69]. In addition, one has to exchange the variance of the noise distribution as well as its skewness and curtosis (3rd and 4th moments).

For a burst gravitational wave search between triggers from resonant-mass and interferometric detectors, we would have to extend this framework in order to include parameters from interferometer ETGs by exchanging information about the frequency band over which an event stretches.

By using the higher order moments, Bienayme's inequality [48] allows an estimate of the false alarm probability and detection efficiency of each event, as a funcion of the corresponding SNR [65], [66]. Although the Bienamye's inequality is a non-parametric test which gives a very conservative estimate of the false alarm probabilities, it provides more statistical robustness in the presence of non-stationary and/or non-gaussian noise.

However, in order to perform such a trigger-based coincidence search between resonant-mass and interferometric gravitational wave detectors, we would have to fully characterise the different search algorithms so that we could exchange

homogeneous definitions of signal parameters such as amplitude and SNR. So one needs to perform Monte Carlo simulations where the effect of each burst search pipeline on particular signal templates is studied. Such simulations and software signal injections in the detector noise are currently being done by the LIGO Burst Analysis Group and the AURIGA group.

Another approach to this method could be to apply a new burst search algorithm that restricts interferometer search to resonant-mass detector's band and apply the optimal filter for the resonant-mass detector. This way, we ensure that the same quantities are compared when searching for coincidences. The required filter should express the amplitude of an event observed by an interferometer in terms of one observed by a resonant-mass detector. However, such techniques are not straightforward and beyond the purpose of this paragraph.

4.2 Externally triggered search

The basic idea which lies beneath the second method of multi-detector burst search is to use a detector with less triggers (such as gamma ray bursts and resonant-mass detectors) to trigger the cross-correlation of data from detectors with a high trigger rate (such as the current interferometeric detectors). This is the externally triggered search laid out in Finn, Romano and Mohanty [68].
For this search, the cross-correlation statistic of the output of two gw detectors is calculated for a time window T when a trigger is observed. That is, one calculates the quantity

$$X = \int_0^T \int_0^T dt dt' x_1(t_{1,\gamma} - t) Q(|t - t'|) x_2(t_{2,\gamma} - t') \ , \tag{4.1}$$

where T is the time window around a bar trigger within which a trigger is expected in the interferometer and Q is the filter kernel. The details concerning the latter filter are discussed in [68]. Here x_α and $t_{\alpha,\gamma}$ are the data samples and the arrival time of the bar trigger for the α-th detector respectively.
This quantity is calculated also for periods of time in which no bar triggers are observed. A statistically significant difference between *on*- and *off*-source correlations indicates the presence of a signal. Finn, Romano and Mohanty suggested the use of Student's t-test as a statistical tool for the difference between the two distributions. However, for the sake of robustness, Tricarico *et al.* [70] recommended the use of the Mann-Whitney u-test, which is useful for systems affected by unmodelled noise backgrounds and/or quasi-stationary noises. The u-test only demands

that the shapes of the two distributions (*off* and *on* populations) are identical and that the two statistical samples are independently drawn. If the requirements of the Mann-Whitney test are met, then the one-tailed z-test can be applied on its outcome u.

4.3 Cross correlation

To fully exploit the network sensitivity, we can resort to a standard technique: the linear time-domain cross-correlation. This is particularly true in the case of events occurring simultaneously on two different detectors.

Such approach is the base of a coherent consistency test on the coincident triggers produced by LIGO ETGs [71]. In fact, the LIGO interferometers have similar sensitivity curves and a relatively small mis-alignement: when coping with similar waveforms, the method is greatly simplified.

Cross-Correlation for coherent analysis of coincident event is a *blind search*, in fact, it makes no *a priori* assumptions on the incoming gravitational signal waveform. Furthermore, it allows suppression of false events without reducing the detection efficiency of the pipeline.

Given two finite series $\{x_i\}$ and $\{y_i\}$ with $i = 1, ..., N$, we recall the well-known linear correlation coefficient r as:

$$r = \frac{\sum_{i=1}^{N} (x_i - \bar{x})(y_i - \bar{y})}{\sqrt{\sum_{i=1}^{N} (x_i - \bar{x})^2} \sqrt{\sum_{i=1}^{N} (y_i - \bar{y})^2}}. \tag{4.2}$$

This latter quantity measures the degree of correlation between the two time series: a value $|r|$ close to unity means a complete correlation (or anti-correlation); while a value $|r|$ close to zero means that the two series are uncorrelated.

Two hypotheses : $\mathcal{H}_0$, ($\{x_i\}$ and $\{y_i\}$ are **uncorrelated**); $\mathcal{H}_1$ ($\{x_i\}$ and $\{y_i\}$ are **correlated**). In case of null hypothesis, the r-statistic is normally distributed around zero, with standard deviation $\sigma = 1/\sqrt{N}$, N being the degrees of freedom. The significance S of null hypothesis is the probability that $|r|$ is larger than what actually measured in case of $\mathcal{H}_0$: S turns out to be

$$S = erfc\left(|r|\sqrt{\frac{N}{2}}\right), \tag{4.3}$$

where $erfc$ is the Complementary Error Function [1].
The Confidence C on the rejection of $\mathcal{H}_0$, i.e. on retaining $\mathcal{H}_1$, is then:

$$C = -\log_{10}(S). \tag{4.5}$$

4.4 Coherent network search

Finally, we discuss the coherent network search method. With this method, the outputs from all the detectors in the network are linearly and coherently combined using their phase information: either by maximizing a network likelihood for the presence of a specified signal in the different data streams or by an excess power search. If noise from the individual detectors of the network are not correlated, then the probability of observing a specific set of data on the different detectors is simply proportional to the sum of the log-likelihood ratios of each detector. The method can be seen as a vector matched filter and, under the assumption of gaussian noise, the coherent analysis can be made optimal in the sense of Wiener filter theory.

4.4.1 Network geometry

We adopt the following reference frames:

- a network frame ($\mathbb{X}$,$\mathbb{Y}$,$\mathbb{Z}$), centered on Earth: the $\mathbb{Z}$ axis aligned along the geographical north, the $\mathbb{X}$ axis pointing at the Γ point of Aries and $\mathbb{Y}$ chosen to have a left-hand frame. Any source direction in the sky is then found through the polar angles (θ,ϕ);

- local frames $(X_\alpha, Y_\alpha, Z_\alpha)$, which are the coordinate frames attached to the detectors of the network. For bar detectors, we choose $\hat{\mathbf{n}}$ unit vector along the bar axis, while for interferometers $\hat{\mathbf{m_1}}$ and $\hat{\mathbf{m_2}}$ unit vectors lying along the arms;

- wave frame, which has the Z_w axis aligned along the propagation direction of the wave. X_w and Y_w are the axes of the polarization (Ψ) ellipse of the wave. We then introduce the wave tensor, W_{ij}.

[1]
$$erfc(x) = \frac{2}{\sqrt{\pi}} \int_x^\infty e^{-t^2} dt \tag{4.4}$$

Rotations of coordinates from one frame to the other are expressed by means of the Euler angles of an orthogonal rotation matrix $\mathcal{O}(\theta, \phi, \psi)$:

$$\begin{aligned} \mathbf{x}_\alpha &= \mathcal{O}\left(\phi_\alpha, \theta_\alpha, \psi_\alpha\right) \cdot \mathbf{x}_{network} \\ \mathbf{x}_w &= \mathcal{O}\left(\theta, \phi, \Psi\right) \cdot \mathbf{x}_{network}, \end{aligned} \tag{4.6}$$

where ϕ_α, θ_α and ψ_α are the Euler angles between the local and the network frames; given the detector latitude λ and longitude β, the orientation ψ_α, the earth angular velocity $\omega_\otimes$ and the Universal Time Coordinate t_{UTC}, these angles can be written as:

$$\begin{cases} \theta_\alpha = \omega_\otimes t_{UTC} \\ \phi_\alpha = \pi/2 - \beta \end{cases} \tag{4.7}$$

Similarly, θ, ϕ and Ψ are the Euler angles between the wave and the network frames; these angles are directly related to the source coordinates Right Ascension RA and declination δ through the relations:

$$\begin{cases} \theta = \delta + \pi/2 \\ \phi = R.A. - \pi/2 \end{cases} \tag{4.8}$$

As the gw signal at α-th detector is the projection of the gw wave tensor over the detector tensor, we write the geometrical factor, the so-called beam pattern function of α-th detector as:

$$s^\alpha\left(\theta, \phi, \Psi\right) = \begin{cases} n^i n^j W_{ij} & \text{(for bars)} \\ \left(m_1^i m_1^j - m_2^i m_2^j\right) W_{ij} & \text{(for interferometers)} \end{cases} \tag{4.9}$$

The detector output $X_\alpha(t_i)$ is then a function of the signal template f_α and the the antenna pattern s_α, and is given by:

$$X^\alpha\left(t_i\right) = A s^\alpha\left(\theta, \phi, \Psi\right) f^\alpha\left(t_i - t_0 - \frac{\hat{\mathbf{r}^\alpha} \cdot \hat{\mathbf{k}}}{c}\right). \tag{4.10}$$

where A is the wave amplitude, $s^\alpha\left(\theta, \phi, \Psi\right)$ is the previously defined beam pattern function, and f^α is the gw waveform convoluted with the detector transfer function; the function is time-shifted of the delay at the α-th detector with respect to the Network frame.

4.4.2 Template-based search

We begin calculating the log-likelihood function Λ of the network with respect to an impulsive plane wave of amplitude A impinging the detectors, then we look for

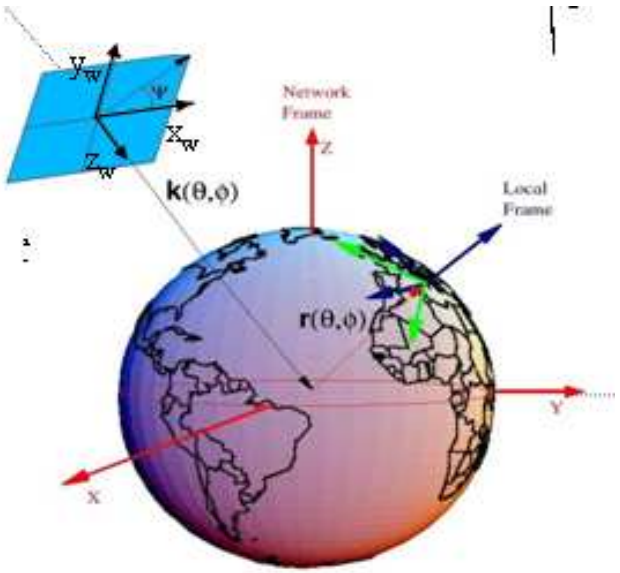

Figure 4.2: Reference frames: 1) the incoming wave reference frame, 2) the detector local frame and the earth centered network frame.

the minimum value of Λ over the burst gravitational wave parameters. This is equivalent to the χ^2 statistic of the data of the detectors in the network obtained by a fit to a given planar gravitational wave burst. The network log-likelihood is given by

$$\chi^2 \equiv \Lambda(A, t_0, \hat{\mathbf{k}}, \Psi) = \frac{1}{2} \sum_{\alpha=1}^{N} \sum_{i,j}^{M_N} \mu_{\alpha,ij} \left[x_\alpha \left(t_i \right) - X_\alpha \left(t_i \right) \right] \left[x_\alpha \left(t_j \right) - X_\alpha \left(t_j \right) \right], \quad (4.11)$$

where $\mu_{\alpha,ij}$ is the inverse of the cross-correlation matrix of the α-th detector noise, $x_\alpha(t_i)$ is the data set of length M_N to be searched for the signal template. For any given sky direction $\hat{\mathbf{k}}$, arrival time t_0 and polarization Ψ , the logarithmic likelihood of the network has to be minimized. It can be shown that Λ reaches a minimum when the amplitude A is simply the weighted sum of the optimal estimates on the single detectors [62]

$$\begin{cases} A_{opt} \left(t_0, \vartheta, \varphi, \Psi \right) = \sum\limits_{\alpha=1}^{N} \frac{A_\alpha(t_0,\vartheta,\varphi,\Psi)}{\sigma_\alpha^2} \Big/ \sum\limits_{\alpha}^{N} \frac{1}{\sigma_\alpha^2} \\ \\ \sigma_\alpha = \left(\frac{1}{2\pi} \int\limits_{-\infty}^{+\infty} \left| f_\alpha \left(\omega \right) \right|^2 / S_\alpha \left(\omega \right) \ d\omega \right)^{-1/2}, \end{cases} \quad (4.12)$$

where σ_α is the standard deviation of the noise in the α-th detector and $S_\alpha(\omega)$ is the spectral density of the noise. From the above equation, one can see that the weighted sum automatically selects which detector in the network to consider in the analysis. This procedure would reduce the contribution of less sensitive detectors, as far as the signal template is concerned.
To properly determine the amplitude, arrival time and χ^2 estimators, we have to assume that the detector noise is a linear superposition of deterministic signals, either gw or environmental events, and quasi-stationary noise. The gaussianity of the data can be checked *a priori* by performing Monte Carlo simulations where signals with known waveforms are injected into the detector noise. The hypothesis testing of signal detection with the network is based on the overall χ^2. The rejection of the null hypothesis is usually achieved by means of a threshold crossing of some signal parameters (eg. amplitude), which corresponds to the sole (and unavoidable) non-linear operation within the framework of the proposed search. The single threshold value will also fix the global false alarm and false dismissal probabilities.

A coherent network search can be set up as follows:

1. Any detector in the network can raise a trigger;

2. All the detector in the network should exchange a short stretch of whitened data $w_{\alpha i}$ around the trigger, together with the adopted whitening filter;

3. For a given template, the χ^2 statistic of the network can be then determined substituting the values calculated in equation 4.12 into the expression

$$\chi^2 = \sum_{\alpha=1}^{N} \frac{\sum_{i}^{M_\alpha} w_{\alpha i}^2}{\varsigma_\alpha^2} - \frac{\left(A_{opt}\left(t_0, \vartheta, \varphi, \Psi\right)\right)^2}{\sigma_{opt}^2} \ , \tag{4.13}$$

   where ς_α and σ_{opt} are the standard deviation respectively of the A_{opt} whitened data $w_{\alpha i}$;

4. Once the likelihood function is calculated, two thresholds (decided through signal injections studies) can be applied to the χ^2 and A_{opt}^2 outcomes, to determine the presence or absence of a genuine gravitational wave signal.

To further test gravitational wave events versus spurious excitations, we can resort to the distinctive properties of the Riemann tensor (transverse and traceless) associated to a planar gravitational wave. It can be shown that there are 3 quantities, the eigenvalues of the polarization tensor W_{ij}, which are invariant

under the group of spatial rotation $\mathcal{O}(3)$ [72]. These quantities are basically the linear, quadratic and cubic combinations of the detector outputs. They are random variables whose distributions can be calculated by means of a Monte Carlo, which uses the noise distributions and orientation information of the individual detectors in the network.

4.4.3 Non-Template search method

As it is extremely difficult to obtain trustful gravitational waveforms, it may be necessary to use blind searches, such as the excess power method [53] or the TFCLUSTER [52]; both of them rely on the same simple concept: one has to compare the power of the data in a given time-frequency domain to the estimated noise power. This kind of search is non-linear but it can be demonstrated to be optimal under the hypothesis that the signal prior is constant [54]. Since these techniques do not require the signal to have a specific form, random noise glitches are much more likely to meet the detection criteria than a signal search such as the matched filter.

A possible implementation of a coherent network gw analysis is to combine all data streams as a *synthetic response* of the network [73], [74]:

$$\mathbf{Y} = \sum_{i}^{N} a_i T(\tau_i)\, \mathbf{y}_i, \tag{4.14}$$

where a_i is a set of real coefficients to be calculated, τ_i are the time shifts of the detectors with respect to the network frame,T is the time-shift operator, $\mathbf{y}_i$ is the data of the i-th detector and N is the number of detectors in the network.

The search algorithm is defined as follows:

1. for any given gw incoming direction θ,ϕ and polarization Ψ, a_i and τ_i are the solutions arising from the minimization of a system of equations constrained to obtain the maximum SNR;

2. with the calculated coefficients the *synthetic response* $\mathbf{Y}$ is formed;

3. the *network power* $P = |\mathbf{Y}|^2$ is then calculated and taken as detection statistic;

4. the largest among all the P-values, which cross a threshold, fixes the energy, the incoming direction and the polarization of the candidate event.

This method is an optimal generalization of the *blind* searches yet developed for single detectors, such as the Excess Power method [53] and TFclusters [52], so that it can process coherently data from a network of detectors.

4.5 Summary and Discussion

The search for coincidence triggers is the most straightforward method one could use to search for burst gravitational waves. This analysis has been widely used in the past and is well understood. However, the problem of comparing homogeneous trigger parameters among interferometers and resonant-mass detectors is quite complex and requires more investigation.

The externally triggered search, on the other hand, would use triggers from resonant-mass detectors to trigger a search in two or more interferometers. It makes no assumption about the waveform of the gravitational wave signal. Moreover, because this search is comparing the statistics of a large number of cross-correlated segments, it is in effect digging into the noise of interferometric detectors.

The Cross-Correlation method has been already applied, as a consistency test, to the data around the events of the three LIGOs, but a generalization to non-parallel detectors with different sensitivity curves is still not accomplished.

The use of a sole threshold makes the coherent network search an extremely powerful method. A single threshold greatly increases the overall efficiency of the network. It overcomes the intrinsic limits connected with the ambiguity of parameter estimation in single detectors and allows for a stronger χ^2 statistical analysis. The efficiency of "OR" logic network is greatly increased with respect to an "AND" logic one, because it allows to detect even those signals which happen to cross the threshold in only one detector in the network, to be detected.

Chapter 5

Conclusions and perspectives

The second AURIGA run is proving the feasibility of a nearly quantum-limited (few hundreds of $\hbar$) gravitational wave detector. The sensitivity and reliability of this second-generation acoustic detector could be compared with the working interferometers' ones.

Moreover, two different analysis pipelines have been implemented in AURIGA data analysis, corresponding to different approaches to the problem of detection:

- the so-called "standard" analysis, which is based on the matched filter to enhance a given waveform in the data stream and make use of devised algorithms to select candidate events and to estimate their parameters;

- the *blind* search, which looks for a power excess in a given time window and rely on a quadratic form of the data as a detection statistic.

The performances of these two pipelines of Event Trigger Generators have been tested on simulated data in case of gaussian stationary noise. Such test has been carried out either for the timing accuracy and the low biases on the estimated amplitudes or for the False Alarms and False Dismissals.

This approach, although simplified, has led to a novel and precise characterization of the two analyses within the framework of the new hardware setup.

However, unless that new hardware upgrades improve the AURIGA detector behavior as for the non-stationarity, both pipelines analyses will suffer from big losses in terms of duty cycle. In fact the analysis will be restricted to well operating periods. Indeed large excesses of false alarms, mainly due to spurious environmental noises, will occur.

As a consequence, the major task to be accomplished is to test the two pipelines in real non-stationary conditions, as regards either the adaptiveness and the robustness of parameters estimation or the characterization of False Alarm rates and False Dismissals.

The encouraging results yet achieved by this initial phase of the new detector AURIGA and the new implementations of data analysis methods will hopefully produce an afterthought on ground-based gw research towards a more coordinated international effort.

In this perspective, multi-detector data analysis methods will soon play a leading role in the gw searches.

This thesis work, far from solving the major problems related to a network data analysis, such as the combination of information from different detectors, is intended to be a brief review of the main possible multi-detector methods. It is of paramount importance that as soon as possible a large international collaboration be set to implement a multi-detector data analysis.

Whether this search will be a simple coincidence analysis among event lists from different detectors, as already done by IGEC for resonant bars [66], or it will have some "flavor" of coherent analysis, is yet not clear, mainly depending on the complexity of the problem, but also on the mutual relationships among the different groups.

Overall the results given in this thesis push towards the implementation of a coherent blind search, which should exploit the full potentials of a network of gw detectors: future work will be devoted to this aim.

Appendix A

ROC (Receiver Operating Characteristic curves)

ROC curves were developed in the 1950's as a by-product of research into making sense of radio signals contaminated by noise, hence the name receiver-operating characteristic. More recently they have been used by medical researchers in decision-making statistics. Central to the idea of ROC curves is the idea of a cutoff level. Let's imagine that we have two statistical populations.

A good algorithm of decision will have both a small fraction false dismissals, FD, as a small fraction false alarms, FA. By varying a threshold on some parameter of a known population, and measuring the error on the outliers, a Receiver Operating Characteristics curve (ROC-curve) is obtained. This curve shows how the fraction of false alarms varies for varying fraction false dismissals. The smaller these fractions are, the more this algorithm is to be preferred. Traditionally the acceptance (1-FD) is plotted versus the FA probability, as shown in figure 1.

Although the ROC curve gives a very good summary of the performance of an algorithm, it is hard to compare two ROC curves. One way to summarize a ROC curve in a single number, is the Area Under the Curve, AUC. This integrates the fraction FA over varying thresholds (or equivalently, varying fraction of FD). Larger values indicate a better separation between target and outliers. Note that for the actual application of the algorithm a specific threshold (or equivalently fraction of FD) has to be chosen. That means, that only one point of the ROC curve is used. It can therefore happen that for a specific threshold an algorithm with a lower AUC might be preferred over another with an higher AUC, but with a larger fraction of FA for that specific threshold.

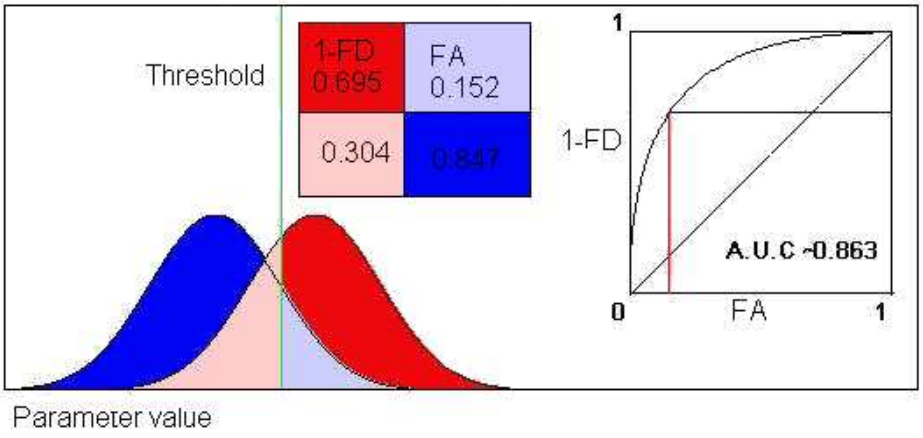

Figure A.1: An example of a ROC curve. Two distributions: target (red) and outliers (blue). Moving the threshold along the parameter axis, you get different fractions of FA and FD: by drawing these ordered couples of values (FA, 1-FD) one produces the ROC curve.

Appendix B

Karhunen-Loève expansion

B.1 Introduction

A well-known result of the theory of integral equations, is that the correlation matrix, $\mathbf{R}$, is bounded, symmetric and positive definite. Thus, it has a spectral decomposition and can be written in terms of its eigenvalues, λ_n, and eigenvectors, φ_n, namely

$$\mathbf{R}_{\alpha\beta} = \sum_{n=1}^{N} \lambda_n \varphi_\alpha^n \varphi_\beta^n \tag{B.1}$$

where N is the dimension of the matrix and

$$\mathbf{R}_{\alpha\beta}\varphi_\beta^n = \lambda_n \varphi_\beta^n \tag{B.2}$$

with the eigenvalues $\lambda_n > 0$. Due to the symmetry and the positive definiteness of the covariance kernel, its eigenfunctions are mutually orthogonal with respect to both the usual inner product and with respect to the inner product derived from the covariance function and form a complete set; if we choose the eigenvectors to be orthonormal, we set a basis in the space $\mathbb{R}^N$ and any data vector lasting less then N samples can be written as

$$\mathbf{x} = \sum_{n=1}^{N} c_n \varphi_n \tag{B.3}$$

which is the so-called discrete Karhunen-Loève Expansion (The expansion was derived independently by a number of investigators (Karhunen, 1947; Loève, 1948; Kac and Siegert, 1947).) [48], [76], [77] and the coefficients, c_n are uncorrelated.

As for the Fourier expansion, which is a special case of KLE, the Parseval's theorem holds,

$$\mathbf{x} \cdot \mathbf{x} = \sum_{n=1}^{N} c_n^2 \tag{B.4}$$

and it is immediate to show that

$$E[c_n c_l] = \lambda_n \delta_{nl} = \sigma_n^2 \tag{B.5}$$

$$E[\mathbf{x} \cdot \mathbf{x}] = \sum_{n=1}^{N} \mathbf{R}_{nn} = \sum_{n=1}^{N} \lambda_n. \tag{B.6}$$

This expansion has been used extensively in the fields of detection, estimation, pattern recognition, and image processing as an efficient tool to store random processes .

Bibliography

[1] R. A. Hulse, Rev. Mod. Phys., **66**, 3, 699-710 (1994).

[2] J. H. Taylor, Rev. Mod. Phys., **66**, 3, 711-719 (1994).

[3] M. Burgay *et al.*, *An increased estimate of the merger rate of double neutron stars from observations of a highly relativistic system*, Nature **426**, 531-533 (2003).

[4] E. Mauceli et al., Phys. Rev. **D 54**, 1264 (1997) and `http://gravity.phys.lsu.edu`.

[5] G. A. Prodi et al, 'Initial Operation of the Gravitational Wave Detector Auriga'. In: *2nd E. Amaldi Conf. on Gravitational Waves, CERN, CH,1-4 July, 1997*, ed. by E. Coccia, G. Veneziano, G. Pizzella (World Scientific, 1998) pp. 148–158 and `http://www.auriga.lnl.infn.it`.

[6] P. Astone et al., Phys. Rev. **D 47**, 362 (1993) and `http://www.roma1.infn.it/rog/explorer/`.

[7] P. Astone et al., Astroparticle Phys. **7**, 231 (1997) and `http://www.roma1.infn.it/rog/nautilus/`.

[8] D. G. Blair et al., Phys. Rev. Lett. **74**, 1908 (1995) and `http://www.gravity.uwa.edu.au/bar/niobe.html`.

[9] Z. A. Allen et al., Phys. Rev Lett. **85**, 5046 (2000) and `http://igec.lnl.infn.it/`.

[10] P. Astone et al., Search for gravitational wave bursts by the network of resonant detectors, *Proc. of the 4th Edoardo Amaldi Conf. on Gravitational Waves (Perth, Western Australia, 8-13 July 2001) Class. Quantum Grav.* **19** (2002), 1367-1375.

[11] K. Danzmann et al., *GEO 600 - Proposal for a 600 m laser-interferometric gravitational wave antenna* (MPQ Garching)(1994) and `http://www.geo600.uni-hannover.de/`.

[12] A. Abramovici et al., LIGO - the laser interferometer gravitational-wave observatory, Science **256**, 325 (1992) and `http://www.ligo.caltech.edu/`.

[13] K. Tsubono, 300 m laser interferometer gravitational wave detector (TAMA300) in Japan, in *Gravitational Wave Experiments*, E. Coccia, G. Pizzella and F. Ronga editors, World Scientific, Singapore (1995) and `http://tamago.mtk.nao.ac.jp/`.

[14] Virgo Final Design 1997 VIR-TRE-1000-13 and `http://www.virgo.infn.it/`.

[15] *LISA - Laser Interferometer Space Antenna*, Esa (1999) and `http://lisa.jpl.nasa.gov/`.

[16] J. P. Zendri *et al*, *Gravitational waves, Proc. 3rd E. Amaldi Conf.* (Caltech, Ca, 1999)ed S. Meshkov (New York: AIP) p 421 (2000).

[17] J. P. Zendri *et al*, *Status report and near future prospects for the gravitational wave detector AURIGA* Class. Quantum Grav. **19** 1925-1933 (2002).

[18] A. Ortolan, *et al.*, in *Proc. of the* 2^{nd} *E. Amaldi Conf. on Grav. Waves (1997)*, eds. E. Coccia, G. Veneziano, G. Pizzella, (World Scientific, Singapore, 1998) p. 204; S. Vitale *et al*, 1^{st} *E. Amaldi Conf. on GW Experiments*, (World Scientific, Singapore, 1995) p. 220.

[19] A. Cesaracciu and G. Vedovato, *A Modular Object Oriented Data Acquisition System for the Gravitational Wave AURIGA Experiment*, proceedings of CHEP03 (2003).

[20] M. Bignotto, *La test facility ultracriogenica per trasduttori di spostamento: sospensioni meccaniche e refrigeratore a diluizione 3He-4He*, degree thesis at the Univ. of Padova, 1999-2000, unpublished (in Italian).

[21] L. D. Landau and E. M. Lifschitz, *Teoria dei Campi*, Editori Riuniti, Roma (1994).

[22] S. Weinberg, *Gravitation and Cosmology*, Wiley & Sons, New York (1972).

[23] C. W. Misner, K. S. Thorne, J. Wheeler, *Gravitation*, San Francisco (1973).

[24] **http://lappc-in39.in2p3.fr/virgo/FrameL/**

[25] S. Bonazzola, J. A. Marck, Astron. Astrophys. **267** 623 (1993).

[26] T. Zwerger, E. Müller, Astron. Astrophys. **320** 209 (1997).

[27] H. Dimmelmeier, J.A. Font, and E. Müller, Astron. Astrophys. **388** 917 (2002).

[28] H. Dimmelmeier, J.A. Font, and E. Müller, Astron. Astrophys. **393** 523 (2002).

[29] C. L. Fryer, D. E. Holz and S. A. Hughes, APJ,**565**, 430 (2002).

[30] K. S.Thorne, in *Three Hundred Years of Gravitation*, S. W. Hawking and W. Israel editors, Cambridge University Press (1987).

[31] C. Cutler and K. S. Thorne, *AN OVERVIEW OF GRAVITATIONAL-WAVE SOURCES*, arXiv:gr-qc/0204090, submitted to World Scientific on April 30, 2002.

[32] È. È. Flanagan and S. A. Huges, *Phys.Rev. D* **57** 4535-4565(1998).

[33] È. È. Flanagan and S. A. Huges, *Phys.Rev. D* **57** 4566-4587(1998).

[34] M. H. P. M. van Putten and E. Ostriker, *Ap. J.***522** L31(2001).

[35] M. H. P. M. van Putten, *Ap. J.***575** L71-74(2002).

[36] M. H. P. M. van Putten and A. Sarkar, *Phys. Rev. D***62** 041502(2000).

[37] C. L. Fryer, S. E. Woosley and D. Hartmann, *Ap. J.* **526** 152 (1999).

[38] M. Shibata, Phys. Rev. **D 60**, 104052 (1999).

[39] C. Kim *et al*, Astrophys. J. **584**, 985-995 (2003).

[40] F. Echeverria, Phys. Rev. D 40 3194 (1989).

[41] L. D. Landau, E. M. Lifshitz, *Theory of elasticity*, Pergamon (1970).

[42] G. Pizzella, *Fisica sperimentale del campo gravitazionale*, La Nuova Italia Scientifica, Roma (1993).

[43] E. Amaldi and G. Pizzella, in *Relativity, Quanta and Cosmology*, F. De Finis editor, Vol. 1 p.5, Johnson Reprint Co., New York (1979).

[44] J. van Paradijs *et al*, *Annu. Rev. Astron. Astrophys.*, **38**, 379.

[45] R. Popham *et al*, *Ap. J.*, **518**, 356 (1999).

[46] M. Cerdonio et al., Cryogenic resonant detectors of gravitational waves: current operation and prospects, in *Gravitation and relativity: at the turn of the millennium*, proceedings of the "GR-15 conference", (Pune - India, 1997), edited by N. Dadhich and J. Narlikar, IUCAA, Pune , pp. 211-230 (1998).

[47] A. Ortolan, *et al.*, in *Proc. of the* 2^{nd} *E. Amaldi Conf. on Grav. Waves (1997)*, eds. E. Coccia, G. Veneziano, G. Pizzella, (World Scientific, Singapore, 1998) p. 204; S. Vitale *et al*, 1^{st} *E. Amaldi Conf. on GW Experiments*, (World Scientific, Singapore, 1995) p. 220.

[48] C. W. Helstrom, *Statistical Theory of Signal Detection*, (Pergamon, Oxford, 1968).

[49] A. Viceré, *Optimal detection of burst events in gravitational wave interferometric observatories*, *Phys. Rev. D* **66** (2002) 062002.

[50] A. Viceré *et al.*, *Testing the performance of a blind burt statistic*,Class. Quantum Grav. **20** S821-S828 (2003).

[51] N. Arnaud *et al.*,*Comparison of filters for detecting gravitational wave bursts in interferometric detectors* ,Phys.Rev. D **67** 062004 (2003).

[52] S. Sylvestre, *Time-frequency detection algorithm for gravitational wave bursts*, **LIGO-P020010-00-D**.

[53] W. G. Anderson, P. R. Brady, J. D. E. Creighton and È. È. Flanagan, Int. J. Mod. Phys. D **9**, 303 (2000).

[54] W. G. Anderson, P. R. Brady, J. D. E. Creighton and È. È. Flanagan, Phys. Rev. D **63**, 042003 (2001).

[55] N. Arnaud *et al.*, Phys. Rev D **65** 042004 (2002).

[56] S. Klimenko, G. Mitselmakher and A. Sazonov, *A cross-correlation technique in wavelet domain for detection of stochastic gravitational waves*, gr-qc/0208007.

[57] A. Ortolan *et al*, *Optimal reconstruction of the input signal in resonant gravitational wave detectors: Data processing algorithm and physical limitations*, *Phys. Rev. D* **50**, 47374743 (1994).

[58] K. L. Bell *et al.*, IEEE TRANSACTIONS ON INFORMATION THEORY, **43**, 2 (1997).

[59] A. J. Weiss and E. Weinstein, IEEE TRANSACTIONS ON ACOUSTICS, SPEECH and SIGNAL PROCESSING, **31-2**, 472-486 (1983).

[60] A. J. Weiss, IEEE TRANSACTIONS ON AEROSPACE AND ELECTRONIC SYSTEMS, **22(6)**, 751-756 (1986).

[61] V. Crivelli-Visconti *et al.*, *Phys. Rev. D* **57**, no.4, 1998, pp.2045-50.

[62] L. Baggio *et al.*, *Phys. Rev. D* **61**, no. 10, 2000, pp. 102001/1-9.

[63] P. Astone *et al.*, *Phys. Rev. D* **12**, no. 12, 1999, pp. 122001/1-6.

[64] P. Astone *et al.*, *Astroparticle Physics* **10**, no. 1, 1999, pp. 83-92.

[65] Z.A. Allen *et al.*, *Phys. Rev. Lett.* **85**, no. 24, 2000, 5046-50.

[66] P. Astone *et al.*, *Phys. Rev. D***68** (2003) 022001.

[67] P. Astone, A. Lobo and B. Schutz, *Class. Quantum Grav.* **11**, no. 8, 1994, pp. 2093-2112.

[68] L. Samuel Finn, S.D. Mohanty and J.D. Romano, *Phys. Rev. D* **60**, no. 12, 1999, pp. 121101/1-4.

[69] IGEC protocol 2000, *http://igec.lnl.infn.it*

[70] P. Tricarico *et al.*, *Phys. Rev. D* **63**, no. 8, 2001, pp. 082002/1-7.

[71] L. Cadonati *Confidence Test for Waveform Consistency of LIGO Burst Candidate Events*, LIGO-G03035-00-Z, presentation at the 5^{th} Edoardo Amaldi Conference on Gravitational Waves.

[72] M. Cerdonio, *et al.*, *Phys. Rev. Lett.* **71**, 1993, 4107-4110.

[73] J. Sylvestre, *Power filters for gravitational wave bursts: network operation for source position estimation*, Proceedings of GWDAW 2002, Class.Quant.Grav. **20** S753-S760 (2003).

[74] J. Sylvestre, *Optimal generalization of power filters for gravitational wave bursts, from single to multiple detectors*, *Phys.Rev. D* **68** 102005 (2003).

[75] I. S. Heng, F. Salemi and A. Ortolan, *Methods for multi-detector burst gravitational wave search*,Class. Quantum Grav. 20 S617-S622(2003).

[76] A. Papoulis, *Probability, Random Variables and Stocastic Processes*, McGraw-Hill, New York (1994).

[77] R. N. Donough and A. D. Whalen, *Detection of Signals in noise*, Academic Press, San Diego (1995).